

Eidgenössische Technische Hochschule Zürich
Swiss Federal Institute of Technology Zurich



Stanford University

A solution-processable artificial solid electrolyte interphase for practical lithium metal batteries

Luca Mondonico
19-945-641

Swiss Federal Institute of Technology (ETH) Zürich
Department of Materials

Supervision

Prof. Dr. Zhenan Bao
Prof. Dr. Markus Niederberger

January 2022

Acknowledgements

First of all, I want to thank Prof. Dr. Zhenan Bao for making this master thesis possible in her group at Stanford University. Special thanks go to my mentor Zhiao Yu for his support and guidance through this thesis. He always had time for explaining and sharing his extensive knowledge on lithium batteries with me. Of course, I want to thank Prof. Dr. Markus Niederberger at ETH Zürich for remotely supporting and supervising me during my visit at Stanford.

Further thanks go to Dr. Weilai Yu for performing XPS analysis of my samples, Dr. Jeffrey Tok who introduced me to lab equipment, and Lily Pay who helped me with administrative matters and kept the lab organized. I thank all Bao battery-subgroup members for providing precious suggestions and continuous feedbacks on my project. Big thanks go to all other Bao Group members for answering smaller and bigger questions and for company during coffee and lunch breaks.

Finally, I express my profound gratitude to my family for providing me with support and continuous encouragement throughout my years of study and through the process of researching and writing this thesis. This accomplishment would not have been possible without them.
Thank you.

Abstract

Li metal is regarded as a promising anode for Li batteries owing to its high specific capacity. However, rapid dendrite growth and low reversibility hinder its practical applications. Building an artificial solid electrolyte interphase (ASEI), which can replace the brittle and inhomogeneous native SEI generated by parasitic reactions between Li and liquid electrolyte, is an effective strategy to stabilize a Li metal anode. In this work, we design and synthesize a multifunctional (mechanically strong, Li^+ ion conductive, electrolyte-blocking, and solution processable) ASEI material, LiAl-FBD, for improving Li metal battery performance. The LiAl-FBD crystal structure demonstrates that Al^{3+} ions are bridged by FBD^{2-} ligands to form anion clusters while Li^+ ions are loosely bound at the periphery, enabling a Li^+ ion conductivity of 9.4×10^{-6} S cm^{-1}. The short yet highly fluorinated ligand chains endow LiAl-FBD with hardness and electrolyte-phobicity. The ASEI was found to effectively prevent Li/electrolyte side reactions and extends the cycle life of Li metal electrodes. Ultimately, by pairing LiAl-FBD coated 50μm-thick Li with industrial 3.5 mAh cm^{-2}, NMC811 cathode, and 2.8 μL mAh^{-1} lean electrolyte, the Li metal full cells show superior cycle life than bare ones, achieving 250 cycles at 1 mA cm^{-2}.

Contents

Acknowledgements **ii**

Abstract **iv**

1 Introduction **1**

2 Theoretical Background **3**

3 Results and Discussion **6**

3.1 Material Design 6

3.2 Mechanical Properties 9

3.3 Li-ion Conduction 9

3.4 Li metal Deposition and Morphology 12

3.4.1 XPS results 12

3.4.2 Li metal deposition 14

3.5 Battery Performance 17

3.5.1 Li | Li symmetric full cells 17

3.5.2 Li-Cu half cells 18

3.5.3 Li-NMC full cells 20

4 Conclusions and Outlook **25**

5 Appendix **30**

5.1 Materials 30

5.1.1 Battery Materials 30

5.2 Methods 31

5.2.1 Synthesis of LiAl-FBD 31

5.2.2 Fabrication of LiAl-FBD coated Li and Cu 31

5.2.3 Nanoindentation tests 32

5.2.4 Material Characterizations 32

5.2.5 Electrochemical Measurements 33

5.3 Supplementary Figures 34

List of Figures

1.1 Conceptual sketch of polymeric Al-FBD network. Blue spheres, Li+ ions; orange spheres, Al atoms; tetrahedra, anion centers; gray chains, soft ligands. 2

3.1 (a) Synthesis of LiAl-FBD. (b) Optical image of LiAl-FBD solution. (c,d) Optical image (c) and refined crystal structure (d) of LiAl-FBD. (e) SEM image of coated LiAl-FBD on Li foil. 7

3.2 (a,b) Nanoindentation measurements showing the Young's modulus (a) and hardness (b) of LiAl-FBD single crystal. (c,d) Polarized optical microscope images showing crystal boundaries of LiAl-FBD coatings on Si wafer. 10

3.3 Impedance evolution of bare Li | bare Li (a) and LiAl-FBD@Li | LiAl-FBD@Li (b) symmetric cells over time. All the cells used 1M LiPF6 in EC/DMC (LP30) + 2% VC + 10% FEC as the electrolyte. 11

3.4 (a-d) XPS of bare Li (a,b) and LiAl-FBD coated Li (c,d) soaked in the carbonate electrolyte for four days. 13

3.5 (a-c) SEM images of Li deposits on bare Cu at different scales. (d-f) SEM images of Li deposits on LiAl-FBD@Cu (underneath the LiAl-FBD coating) at different scales. (g-i) SEM images of LiAl-FBD@Cu (with Li deposits underneath) after 10 (g) or 50 (h,i) cycles in the Li | Cu half cells. (j,k) EDS images showing F (j) and Al (k) element distribution on the Li surface underneath LiAl-FBD coating. (l) EDS image showing Al element distribution for the area in (g). 15

3.6 (a,b) Cycling performance of bare Li | bare Li and LiAl-FBD@Li | LiAl-FBD@Li symmetric cells; note that figure (b) is a portion of figure (a) as to better visualize the overpotential difference. All the cells used 1M LiPF6 in EC/DMC (LP30) + 2% VC + 10% FEC as the electrolyte. 18

3.7 (a) Cycling curves of 50-μm-thick Li | bare Cu and 50-μm-thick Li | LiAl-FBD@Cu half cells using 1M LiPF6 in EC/DMC (LP30) + 2% VC + 10% FEC electrolyte. (b) CEs of Li | Cu half cells in (a). Replicated results for LiAl-FBD@Cu are shown in (b). (c) Aurbach protocol [31, 32] test of Li | bare Cu and Li | LiAl-FBD@Cu half cells showing the average CE. (d) Cycling of 50-μm-thick Li | LiAl-FBD@Cu half cell using 4M LiFSI/DME electrolyte at 1 mA cm^{-2} current density and 3 mAh cm^{-2} areal capacity. (e,f) Cycling of 50-μm-thick Li | bare Cu and 50-μm-thick Li | LiAl-FBD@Cu half cells using LP30 + 2% VC + 10% FEC electrolyte at 1 mA cm^{-2} current density and 3 mAh cm^{-2} areal capacity. 19

3.8 (a,b) Full cell performance and corresponding CE evolution using 50-μm-thick Li, commercial NMC532 cathode sheet, and commercial carbonate electrolyte. (c,d) Full cell performance and corresponding CE evolution using 50-μm-thick Li, industrial NMC811 cathode sheet, and high-concentration ether electrolyte. Replicated results for bare Li and LiAl-FBD@Li cells are shown here, in Fig. 3.8 and Supporting Figures, 5.12. 22

3.8 Long-term cycling of thin-Li | NMC full cells under different conditions. (a,b) 50-μm-thick Li | 2 mAh cm^{-2} NMC532 using LP40 + 10% FEC under C/2 cycling. (c,d) 42-μm-thick Li | 2 mAh cm^{-2} NMC532 using LP57 + 1% VC + 10% FEC under 0.3C cycling. (e,f) 50-μm-thick Li | 3.5 mAh cm^{-2} NMC811 using LP40 + 10% FEC under 0.3C cycling. (g,h) 50-μm-thick Li | 3.5 mAh cm^{-2} NMC811 using 0.6 M LiTFSI + 0.4 M LiDFOB + 0.05 M LiPF6 in FEC/EMC (3/7) under 0.3C cycling. Replicated cells are shown here. 24

5.1 ^{1}H-NMR of LiAl-FBD (upper) and FBD (bottom). 34

5.2 ^{19}F-NMR of LiAl-FBD (upper) and FBD (bottom). 35

5.3 ^{13}C-NMR of LiAl-FBD (upper) and FBD (bottom). 36

5.4 Crystal structure of $Li_3Al_3(FBD)_6(DME)_3$ viewing from a- (a), b- (b), and c- (c) axis [25]. 37

5.5 Nyquist plot of electrochemical impedance of dry and wet LiAl-FBD pellet. The wet pellet was prepared by adding 10 w.t.% DME solvent as the plasticizer into the dry pellet. 37

5.6 (a-c) Top-view SEM images with different scales showing the conformal morphology of LiAl-FBD coating. (d-f) Cross-sectional SEM images showing the thickness (∼500 nm) of LiAl-FBD coating on Li foil. (g-j) EDS of LiAl-FBD coating on 50-μm-thick Li metal foil: Al (h), C (i), and F (j). 38
5.7 Interfacial impedance evolution of bare Li | bare Li and LiAl-FBD@Li | LiAl-FBD@Li symmetric cells over resting time, extracted from Fig. 3.3a and 3.3b. 39
5.8 ^{1}H- (a) and ^{19}F- (b) NMR of the solutions after LiAl-FBD crystal soaking in LP30 or 4M LiFSI/DME electrolytes for ∼24 h. 40
5.9 (a,b) XPS C1s (a) and Li1s (b) of bare Li. (c-e) XPS C1s (c), Li1s (d) and Al2p (e) of LiAl-FBD@Li. 41
5.10 (a,b) SEM images of LiAl-FBD@Cu (with Li deposits underneath) after 10 cycles in the Li | Cu half cell. (c,d) EDS mapping of F (c), and O (d) element. (e,f) SEM images (top-view for e and cross-sectional for f) of LiAl-FBD@Cu (with Li deposits underneath) after 50 cycles in the Li | Cu half cell. Carbonate electrolyte LP30 + 2% VC + 10% FEC was used here. The samples were prepared by cycling 1 mAh cm^{-2} Li at 0.5 mA cm^{-2} current density on either bare Cu or LiAl-FBD@Cu for either 10 or 50 cycles, followed by depositing 1 mAh cm^{-2} Li at 0.5 mA cm^{-2} current density on the Cu substrate (underneath LiAl-FBD coating). 42
5.11 (a,b) Grazing-incidence wide-angle X-ray scattering (GIWAXS) results of LiAl-FBD coating on Si wafer [25]. 43

5.12 Comparison of cycling performance of thin-Li | NMC full cells: bare Li, LiAl-FTEG@Li, and LiAl-FBD@Li. 50-μm-thick Li | 2.6 mAh cm^{-2} NMC811 using LP40 + 10% FEC under 0.5C cycling. Replicated cells are shown here. 44

Chapter 1

Introduction

Lithium metal anodes are regarded as some of the most promising negative electrodes in the next generation of batteries [1, 2]. Unfortunately, lithium metal anode's poor cyclability has so far prevented its use in energy storage devices. The issue originates mainly from the unstoppable parasitic reactions between the highly-reactive Li and the electrolyte components, eventually resulting in a poorly-passivating layer called solid-electrolyte-interphase [3, 4].

To address the issues affecting Li metal anodes, artificial SEIs have recently gained attention as an alternative approach, given their potential compatibility with commercial electrolytes [5] and practical manufacturing processes [6]. Researching a novel solution-based processing for ASEIs on the Li metal anode is tremendously important, as it would allow effective ASEIs implementation in the most common industrial coating methods such like spray coating, gravure printing and slot-die coating.

In this work, we design and synthesize a solution-processable, mechanically strong, Li-ion conductive, and electrolyte-blocking ASEI. The artificial SEI is based on a

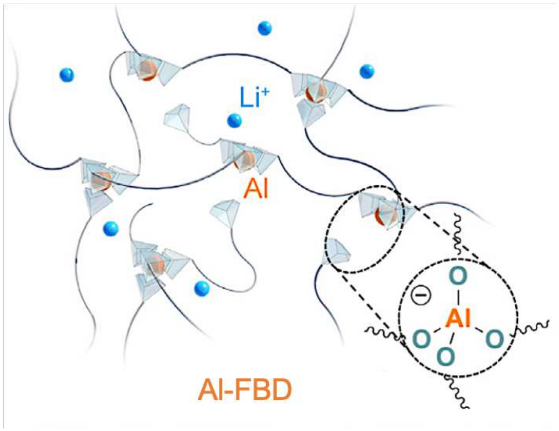


Figure 1.1: Conceptual sketch of polymeric Al-FBD network. Blue spheres, Li+ ions; orange spheres, Al atoms; tetrahedra, anion centers; gray chains, soft ligands.

dynamic polymeric network with high Li^+ single-ion conductivity, whose active centers are tetrahedral $Al(OR)_4^-$ (R = soft fluorinated linker) anions which also act as counter anions to Li^+ ions (Fig. 1.1). With this novel artificial SEI, we demonstrate over 300 stable stripping and plating cycles in Li | Cu cell using commercial carbonate-based electrolyte. Over 90 percent capacity retention for almost 200 cycles in the Li | NMC full battery was achieved using directly-coated thin Li foils and commercial, industry-standard NMC cathode sheets. The design concept of using dynamic single-ion conductor as a stable and scalable artificial SEI is surely promising for practical Li metal batteries.

Chapter 2

Theoretical Background

In recent years, demand for high-density energy storage devices has reached an all-time high [7]. While playing an increasingly significant role in the energy scenario, Li-ion batteries are approaching their theoretical limit [7]. It is therefore essential to develop a new generation of batteries that can meet the increasingly demanding requirements of modern electronic devices such as computers, cell phones and electric cars [8, 9].

Possessing the highest theoretical specific power ($3,860$ mAh g^{-1}) and the lowest electrochemical potential (3.04 V, compared to the standard hydrogen electrode) of any other known negative electrode material, Li metal indeed has the potential to deliver the highest specific energy should it be used as an anode in Li batteries [8, 9].

Despite its great potential, a number of important drawbacks prevent Li metal from being industrially implemented as an anode in Li batteries.
Firstly, Li readily reacts with conventional/commercial carbonate electrolytes to form a so-called solid-electrolyte interface [3, 4], whose typically heterogeneous

nature causes local fluctuations of Li^+ ion flux and current density. The native SEI fails to passivate the Li surface during cycling, thus leading to the creation of dendrites [10]. Secondly, large volume change during Li stripping and plating generates cracks in the mechanically brittle SEI, forms dead Li, and causes further electrolyte consumption [10]. The combined action of the aforementioned effects decreases the Coulombic Efficiency (CE) and compromises the long-term cycle life of Li metal anodes [8].

Several strategies have been proposed to counteract said degradation pathways, including additives and liquid electrolyte engineering [11–14], solid-state electrolytes [4, 15], chemical pretreatment of Li metal [16–18], Li metal hosts [19], or the employment of a shielding cation layer [20]. Nevertheless, obtaining a stable SEI on Li metal is particularly complex [3, 8], thus making the design and fabrication of artificial SEIs a particularly attractive alternative to replace native SEI on Li.

An ideal artificial SEI must possess several essential features. Initially, prior work suggested advantages of having high-modulus coatings on Li [3, 4]; however, Liu at al. observed that in order to achieve macroscopic uniform Li deposition, the SEI needs to readily adapt to the large volume change during Li stripping and plating [10]. This is only possible if the SEI possesses dynamics properties and a certain degree of flowability. Secondly, the artificial SEI should guarantee fast and uniform Li^+ single-ion conductivity as to reduce "hot spots", stabilize the Li metal anode and increase the critical Li deposit size [4, 21].
Lastly, harmful side reactions between lithium and coating or lithium and electrolyte should be minimized; therefore, SEI itself needs to be chemically an electrochemically inert as to mitigate electrolyte penetration in the coating [22].

Nonetheless, only a few SEIs have been implemented that possess all major desirable properties, such as flowability [23], dynamic properties [10], or high ion conductivity [17, 21]. In addition, most of the reported Li metal artificial SEIs, mainly compatible with ether-based electrolytes only, cannot be utilized in current Li-ion batteries due to their incompatibility with commercially used high-voltage and high-energy density lithium nickel manganese copper oxide (NMC) cathodes. It is thus necessary to carefully engineer future artificial SEIs and extend their compatibility to a much broader electrolyte selection.

Despite being challenging, both scientifically and practically, to synergistically incorporate all the ideal properties into one material, it is worth developing a multifunctional ASEI for better protecting Li metal anodes.

Chapter 3

Results and Discussion

3.1 Material Design

Previous work demonstrated the validity of tetrahedral $Al(OR)_4^-$ anions when applied in dynamic polymeric networks for artificial SEIs [24]; therefore, tetrahedral $Al(OR)_4^-$ anions were chosen as dynamic crosslinking centers in our current polymeric architecture. The Li^+ counter ions are introduced as the mobile ions in the network, while relatively soft fluorinated chains (2,2,3,3-tetrafluoro-1,4-butanediol, FBD) are chosen as inert ligands (Fig. 3.1a). Being less chemically reactive and more solvent resistant compared to their non-fluorinated version, 1,4-butanediol (BDO) [24], the FBD chains can potentially mitigate side reactions between Li and the dynamic polymeric network, prevent the dissolution of the network in polar carbonate electrolytes, reduce electrolyte penetration through the ASEI, and guarantee flowability when combined with dynamic $Al(OR)_4^-$ crosslinking sites. Most important, Li^+ ions, which are directly introduced during the polymeric structure synthesis, can transport through the network of fixed $Al(OR)_4^-$ anions, thus making the ASEI a solid-state single-ion conductor [5].

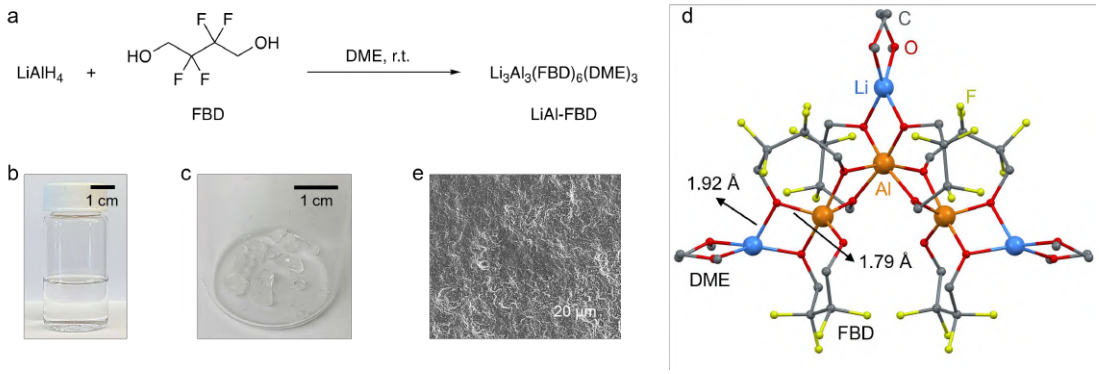


Figure 3.1: (a) Synthesis of LiAl-FBD. (b) Optical image of LiAl-FBD solution. (c,d) Optical image (c) and refined crystal structure (d) of LiAl-FBD. (e) SEM image of coated LiAl-FBD on Li foil.

LiAl-FBD, the key component for the artificial SEI, is derived from the instant reaction between $LiAlH_4$ and FBD in 1,2-dimethoxyethane (DME). After the reaction, which released H_2 as the sole by product, the deprotonation of FBD was confirmed by nuclear magnetic resonance (NMR) spectroscopy. The obtained species, $LiAl(FBD)_2$ in simplified formula, is soluble in DME to form a transparent solution (see Fig. 3.1b), being thus suitable for use in common solution-based coating processes. After evaporating the solvents, crystals are produced (Fig. 3.1c), whose size ranges from centimeters to millimeters; however, it is possible to obtain smaller single crystals upon controlled evaporation of limited amounts of solvent.

By single crystal X-ray diffraction (SCXRD), the crystal structure can be solved and further refined to be $Li_3Al_3\,(FBD)_6\,(DME)_3$ [25]. As shown in Fig. 3.1d, the crystal structure comprises of an anion cluster composed of three Al^{3+} cations as the centers and six deprotonated FBD^{2-} as the bridges/ligands linking those Al^{3+} centers. The ^{1}H- and ^{19}F-NMR spectra also indicate such a multi-state or clustering feature by showing broadened peaks after the synthesis (Supplementary Figures 5.3, Fig. 5.1, 5.2 and 5.3). It is worth noting the three Li^+ ions are lo-

cated at the periphery of the cluster, chelated by one DME solvent molecule for each. The longer distance between oxygen atoms on deprotonated FBD^{2-} with Li^+ (1.92Å) compared to Al^{3+} (1.79Å) clearly suggests their loose coordination with Li^+ yet stronger binding with Al^{3+} [25]. As proved by the ASEI high ionic conductivity (up to 9.4×10^{-6} S cm^{-1} at room temperature; see Supplementary Figures 5.3, Fig. 5.5), such an essential feature frees mobile Li^+ ions, and enables reasonably fast ion transport through the ASEI when applied on Li metal surface. In addition, compared to previous research using longer ligands [5], the short yet highly-fluorinated FBD ligand not only prevents Li^+ depletion by providing higher Li^+ concentration (2 w.t.% for LiAl-FBD versus 0.8 w.t.% in the previous report [5]) in the ASEI, but also manifests pivotal electrolyte-blocking properties.

Finally, LiAl-FBD feasibility as a crystalline coating layer was confirmed by scanning electron microscopy (SEM). As shown in Fig. 3.1g and in Supplementary Figures 5.3, Fig. 5.6, a conformal protection layer with a thickness of ~ 500 nm was observed on a thin Li foil. The crystalline nature of LiAl-FBD coating was supported by polarized optical microscope and grazing-incidence wide-angle X-ray scattering (GIWAXS) [25] (Supporting Figures, Fig. 5.11).

It is also worth remarking the LiAl-FBD ASEI was successfully implemented on Li foil using dip-coating method from the solution (5.2.2), thus showing the potential compatibility of our proposed ASEI with solution-based large-scale processing methods.

3.2 Mechanical Properties

It has been previously demonstrated the importance of mechanic properties in improving Li deposition in artificial SEI materials [5, 26].

The strength of crystalline LiAl-FBD was thus assessed via nanoindentation test [27]. As can be seen in Fig. 3.2e and 3.2f, LiAl-FBD displayed a Young's modulus of $\sim 30 - 40$ GPa (in the stable region) and hardness (> 2 GPa (in stable region), both moduli being considerably higher than those of previously reported polymer ASEIs [28, 29]. Previous studies hypothesized a Young's modulus of 4 GPa to be usually effective for a successful suppression of Li dendrites [26, 27], thus making mechanical strength a property of key importance for LiAl-FBD ASEIs to protect Li metal anodes.

3.3 Li-ion Conduction

High Li^+ ion conductivity and high Li transference number (LTN) are notoriously beneficial in artificial SEI to help increase the critical Li nucleate size, render smooth Li deposition, and reduce parasitic reactions of anions with Li metal [4, 21]. A comprehensive understanding of the main Li^+ ion transport mechanism inside ASEI is therefore necessary.

In previous studies [5], molecular dynamics (MD) simulations on polymeric networks similar to LiAl-FBD were performed to better explain the ion transport behavior inside the ASEI. In these cases, the dynamic artificial SEI was simulated as a network of uniformly distributed Li atoms, Al centers, and FTEG (1H,1H,11H,11H-perfluoro-3,6,9-trioxaundecane-1,11-diol, FTEG) polymeric ligand chains. It was hypothesized the presence of two different Li solvation en-

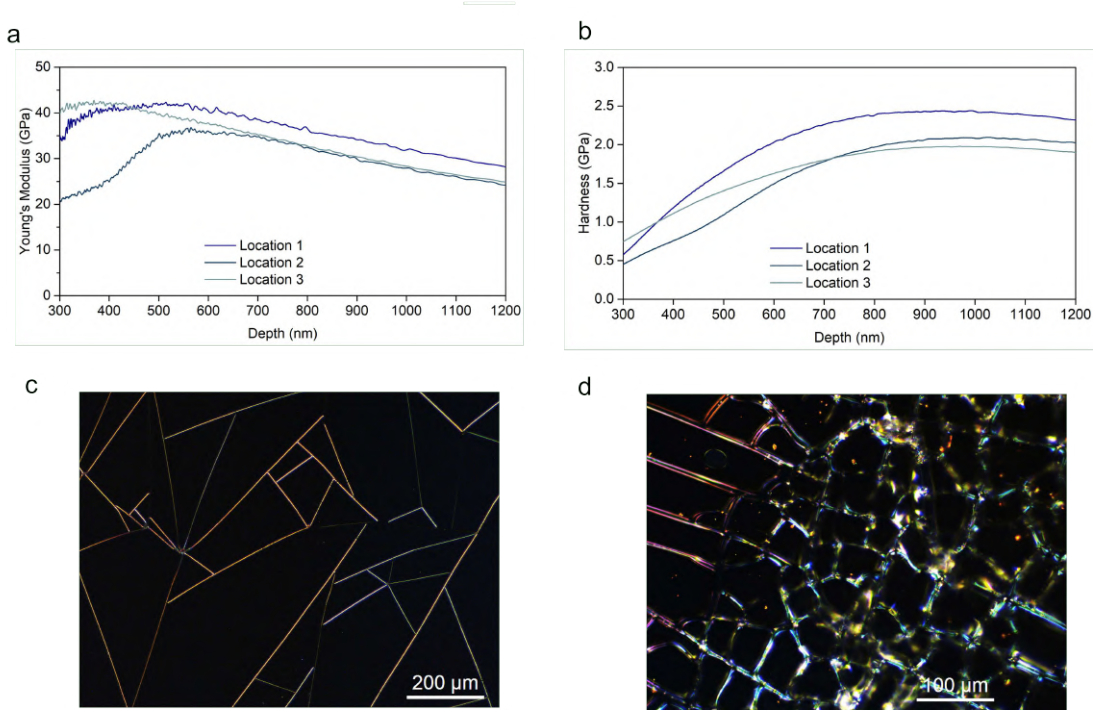


Figure 3.2: (a,b) Nanoindentation measurements showing the Young's modulus (a) and hardness (b) of LiAl-FBD single crystal. (c,d) Polarized optical microscope images showing crystal boundaries of LiAl-FBD coatings on Si wafer.

Note: Clear and straight crystal grain boundaries indicate the crystalline nature of LiAl-FBD coating.

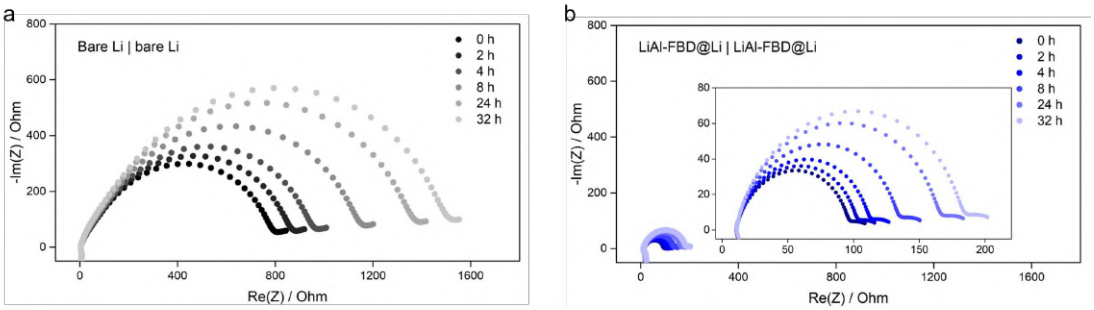


Figure 3.3: Impedance evolution of bare Li | bare Li (a) and LiAl-FBD@Li | LiAl-FBD@Li (b) symmetric cells over time. All the cells used 1M LiPF6 in EC/DMC (LP30) + 2% VC + 10% FEC as the electrolyte.

vironments in the polymeric ASEI: one is from Li^+ ions coordinated close to the $Al(OR)_4^-$ center, and the other is from Li^+ ions coordinated by the ligand chains. Ultimately, it was proved by experimental and simulation results the transport of Li^+ ions in the ASEI is mainly assisted by the fluorinated ligand chains [5]. It is therefore reasonable to assume that Li^+ ion transport through our proposed LiAl-FBD ASEI occurs via FBD-mediated hopping between Al centers.

To further investigate the Li-ion conduction feature of our ASEI, electrochemical impedance spectroscopy (EIS) measurements were performed. LiAl-FBD ASEI impedance is proved by EIS to be much lower compared to bare sample one. As shown by the EIS Nyquist plots (Fig. 3.3a and 3.3b; Supplementary Figures 5.3, Fig. 5.7), the LiAl-FBD protected Li | Li symmetric cell maintained low and stable interfacial impedance over the whole cell resting time, i.e. only increasing from $\sim 100\ \Omega$ to $\sim 180\ \Omega$; by contrast, the bare Li | Li symmetric cell showed continuous and drastic increase in impedance from immediately after the cell assembling ($\sim 800\ \Omega$) to 32 h ($\sim 1,500\ \Omega$). As expected, a consistently high interfacial impedance was generated by the poorly conductive and devastated natural SEI, which originates from continuous electrolyte consumption [3, 8].

3.4 Li metal Deposition and Morphology

To understand more about the protective effect resulting from the LiAl-FBD coating, we conducted X-ray photoelectron spectrometry (XPS) along with SEM analysis to study the ASEI performance, shape and Li deposition morphology, respectively.

3.4.1 XPS results

XPS measurements for the LiAl-FBD ASEI are also performed. To prevent collateral effects from residual salts or LiAl-FBD coating itself, the samples were washed using water and anhydrous DME to expose a fresh surface prior to XPS and SEM testing.

For the bare Li metal, high contents of inorganic electrolyte-derived substances were seen (Fig. 3.4a and 3.4b). For instance, $Li_xPO_yF_z$ ($\sim$ 687 eV, F1s; $\sim$ 58 eV, Li1s; $\sim$ 535 eV, O1s) and LiF ($\sim$ 56 eV, Li1s) are the decomposition products of $LiPF_6$ salt ($\sim$ 690 eV, F1s), whereas Li_2CO_3 ($\sim$ 533 eV, O1s) and Li_2O are the ones derived from carbonate solvents. Moreover, the species vastly varied with depth profiling, suggesting that such a vertically-nonuniform feature along with the severe electrolyte degradation may be responsible for the poor performance of bare Li. By contrast, XPS spectra of LiAl-FBD@Li revealed distinct patterns showing FBD-based species dominating both F1s and O1s spectra (Fig. 3.4c and 3.4d). Electrolyte-decomposed products were not observed with LiAl-FBD protection, indicating its excellent electrolyte-blocking capability. Although LiF is also present within LiAl-FBD coating Li (Fig. 3.4d), it's uniformly distributed across various levels. Indeed, the LiF species may primarily stem from well-controlled reactions [5] between FBD ligands and Li metal, and such a vertical uniformity

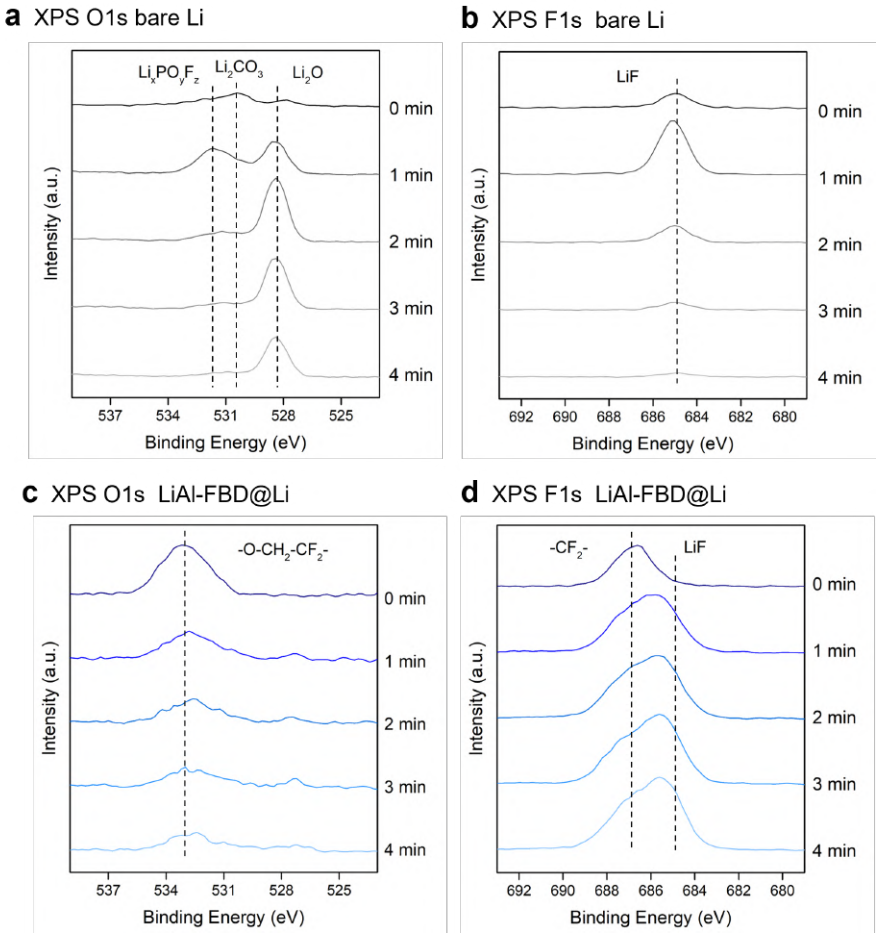


Figure 3.4: (a-d) XPS of bare Li (a,b) and LiAl-FBD coated Li (c,d) soaked in the carbonate electrolyte for four days.

was proved to be beneficial to Li metal cyclability [18, 30]. The XPS of other elements further supported our argument (Supplementary Figures 5.3, Fig. 5.9).

Overall, the previous results clearly indicate that the LiAl-FBD is effective in mitigating the electrolyte penetration and preventing continuous reactions between Li and electrolyte, which typically occur in the uncoated Li.

3.4.2 Li metal deposition

Li deposition morphology is an important factor that determines Li metal stability to ASEI protection. As suggested by previous literature [13], higher Li metal battery performance can be achieved if Li grows on the current collector in a non-dendritic fashion.

In order to better understand the origins of the LiAl-FBD-coated Li metal improved cyclability, we thus performed SEM imaging of Li metal morphology on the Cu current collector. It was noted that the LiAl-FBD protection layer remained nearly intact after 1 mAh cm^{-2} Li deposition, despite being deliberately peeled off to allow cross-sectional SEM analysis (Supplementary Figures 5.3, Fig. 5.10). In order to better study the Li deposition morphology, we then washed off the top protective LiAl-FBD coating.

With the LiAL-FBD protection, the deposited Li at 1 mAh cm^{-2} predominantly showed flat and chunky 2D plate-like structures (Fig. 3.5d, 3.5e and 3.5f); on the other hand, the Li deposits for the bare Cu sample appeared the be needle-like or small particles (Fig. 3.5a, 3.5b and 3.5c), as would be expected with carbonate electrolytes [5]. To clearly show the difference (dendrites versus chunky grains), carbonate electrolyte LP30 + 2% VC + 10% FEC was used here. The samples were prepared by depositing 1 mAh cm^{-2} Li at 0.5 mA cm^{-2} current density on

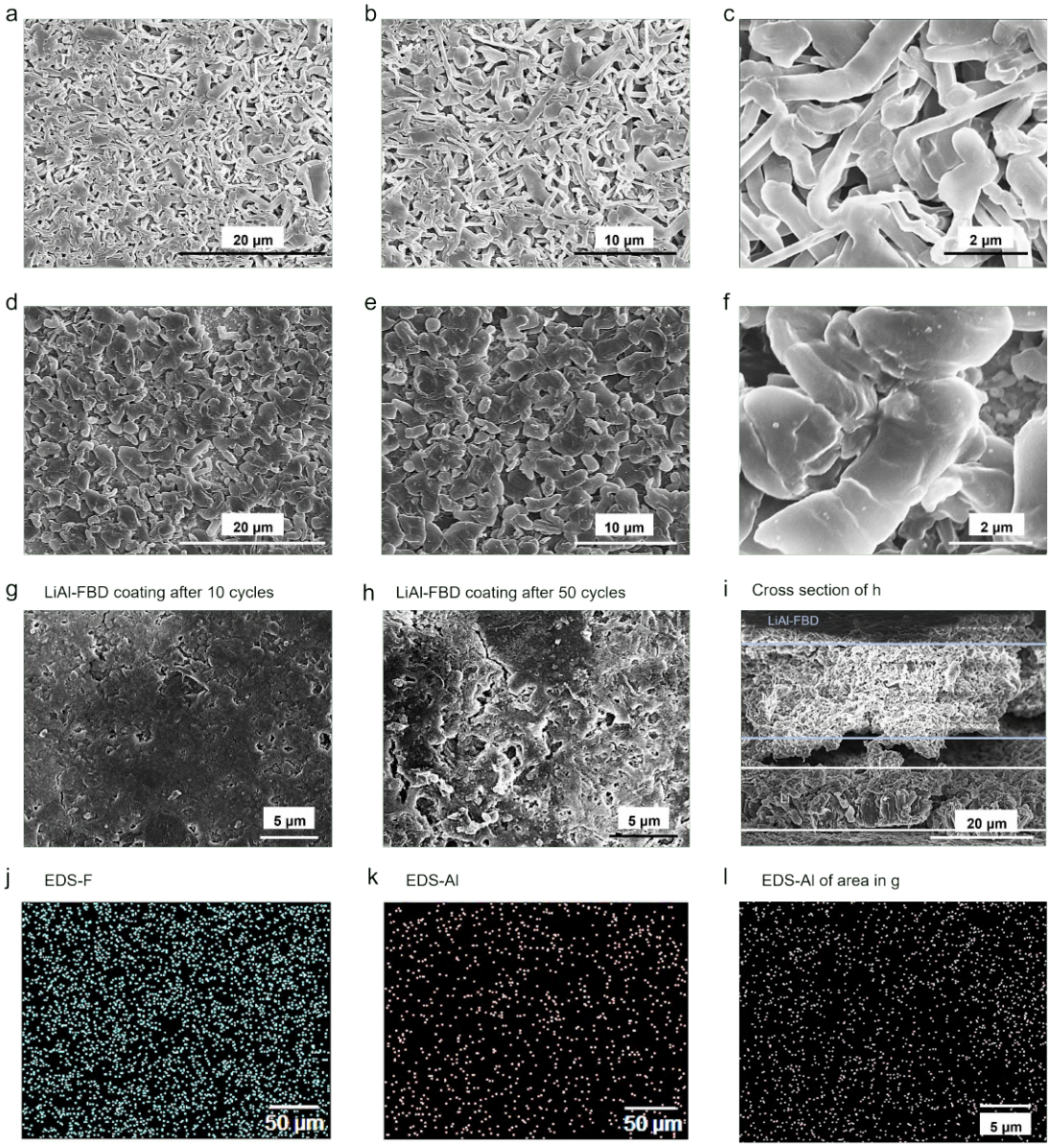


Figure 3.5: (a-c) SEM images of Li deposits on bare Cu at different scales. (d-f) SEM images of Li deposits on LiAl-FBD@Cu (underneath the LiAl-FBD coating) at different scales. (g-i) SEM images of LiAl-FBD@Cu (with Li deposits underneath) after 10 (g) or 50 (h,i) cycles in the Li | Cu half cells. (j,k) EDS images showing F (j) and Al (k) element distribution on the Li surface underneath LiAl-FBD coating. (l) EDS image showing Al element distribution for the area in (g).

either bare Cu or LiAl-FBD@Cu, followed by washing with anhydrous DME solvent to remove residue electrolyte and the coating layer.

The energy-dispersive X-ray (EDS) spectra showed uniformly distributed F and Al elements on the Li metal deposits surface although DME solvent washed most of the LiAl-FBD coating off (Fig. 3.5j and 3.5k). This not only confirms the planarly uniform distribution of LiAl-FBD coating, but also validates the XPS Al2p results by showing good contact between the ASEI and Li metal layer (Supplementary Figures 5.3, Fig. 5.9e).

Although after long cycling the LiAl-FBD coating layer disintegrated and became less conformal, the coating was still found to adhere to the surface of almost each Li deposit, serving as a functional ASEI (Fig. 3.5g, 3.5h and 3.5i; Supplementary Figures 5.3, Fig. 5.10). Particularly, as shown in Fig. 3.5i and Fig. 5.10f, the Li deposits (after 50 cycles) were densely packed underneath the LiAl-FBD layer (top part between the light blue lines and the layer was curled up due to peeling), confirming its protection effect even after long-term cycling.

The least Li | Li interfacial impedance evolution over time (Fig. 3.3b) and the fewest products of parasitic reactions between Li and electrolyte (Fig. 3.4c), further demonstrate the superior Li-surface protection effect of the LiAl-FBD coating is a critical factor for improving the Li deposition morphology. By contrast, the continuous increase observed in Li | Li impedance bare Li (Fig. 3.3a) along with the lack of conformal protection is responsible for its worse Li deposition morphology. These SEM observations are consistent with the Li | Cu cycling results (Fig. 3.7a and 3.7b) and confirm that the efficient design of LiAl-FBD improves Li growth morphology.

3.5 Battery Performance

After verifying its suitability as a conformal ASEI, LiAl-FBD coating was investigated in batteries to confirm its effectiveness in Li metal protection. Conventional carbonate-based electrolyte 1 M $LiPF_6$ in ethylene carbonate (EC) / dimethyl carbonate (DMC) (denoted as LP30) + 2% vinylene carbonate (VC) + 10% fluoroethylene carbonate (FEC) was chosen; therefore, it was possible to examine the effectiveness of LiAl-FBD coating in an electrolyte which is not only commercial, scalable and low-cost, but also not typically compatible with Li metal.

3.5.1 Li | Li symmetric full cells

Firstly, Li | Li symmetric cells were used to examine the electrolyte-blocking feature with LiAl-FBD coating. As already predictable from the EIS evolution over time, the cycling behavior of LiAl-FBD coated Li | Li symmetric cell is far more stable than bare Li one (Fig. 3.6a). The coated cell was cycled for more than 1000 h (500 cycles) without significant polarization or short circuiting, while the bare Li cell experienced severe overpotential increase after cycling for only $\sim$ 300 h, followed by failure at $\sim$ 460 h. In addition, the cycling overpotential value is $\sim$ 25 mV and $\sim$ 100 mV for LiAl-FBD@Li and bare Li, respectively, demonstrating a four-time lower polarization for the protected Li (Fig. 3.6b). These results prove the effectiveness of LiAl-FBD in preventing the Li metal corrosion caused by liquid electrolytes. Combined with the high ionic conductivity of the ASEI, stable impedance and cycling of Li metal anodes can be achieved.

To further confirm the electrolyte-phobic nature of our ASEI, a soaking experiment was conducted: a LiAl-FBD crystal was immersed in either the carbonate (LP30) or ether electrolyte (4M LiFSI/DME 27) used in this work; ^{1}H- and ^{19}F-NMR

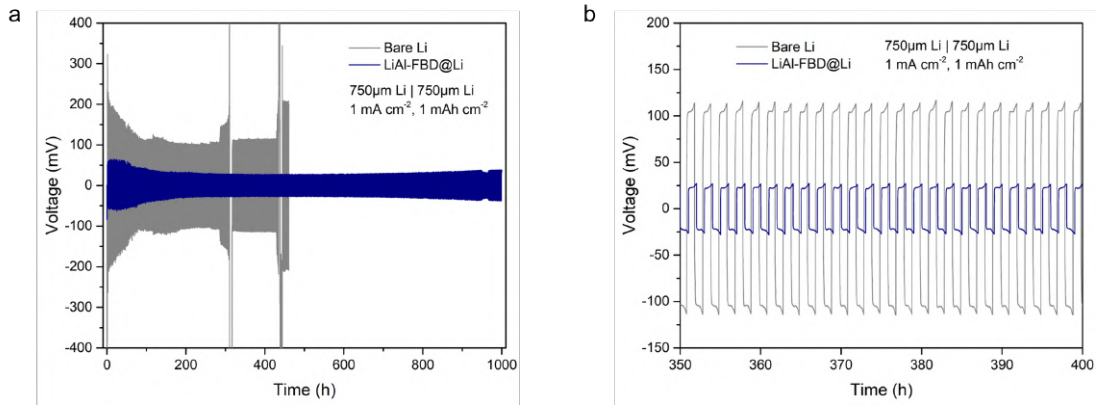


Figure 3.6: (a,b) Cycling performance of bare Li | bare Li and LiAl-FBD@Li | LiAl-FBD@Li symmetric cells; note that figure (b) is a portion of figure (a) as to better visualize the overpotential difference. All the cells used 1M LiPF6 in EC/DMC (LP30) + 2% VC + 10% FEC as the electrolyte.

were performed after 24 h, and they indicated negligible dissolution of LiAl-FBD species (Supplementary Figures 5.3, Fig. 5.8).

3.5.2 Li-Cu half cells

Li | Cu cells were also studied to show the impact of LiAl-FBD coating on cycling stability and Li metal CE. In contrast with the thick Li foils used in Li | Li symmetric cells, the practical, industrial 50-μm-thin Li was here used to assess the practicality of implementing LiAl-FBD coating in realistic battery structures. As suggested by the the voltage curve in Fig. 3.7a, severe fluctuation occurred in the Li | bare-Cu cell, especially during the initial and final stage of cycling; this further confirms the poor passivation capability of native SEI generated by liquid electrolyte. On the contrary, the Li | LiAl-FBD@Cu cell showed a more stable cycling plateau and longer cycle life than the bare Cu one, validating the LiAl-FBD protection for Li metal cycling. As expected, the extracted CEs of two replicated Li | LiAl-FBD@Cu half cells (filled and hollow blue dots in Fig. 3.7b) are consistently high (>97.5%). It can be also noted a slightly higher CE for the

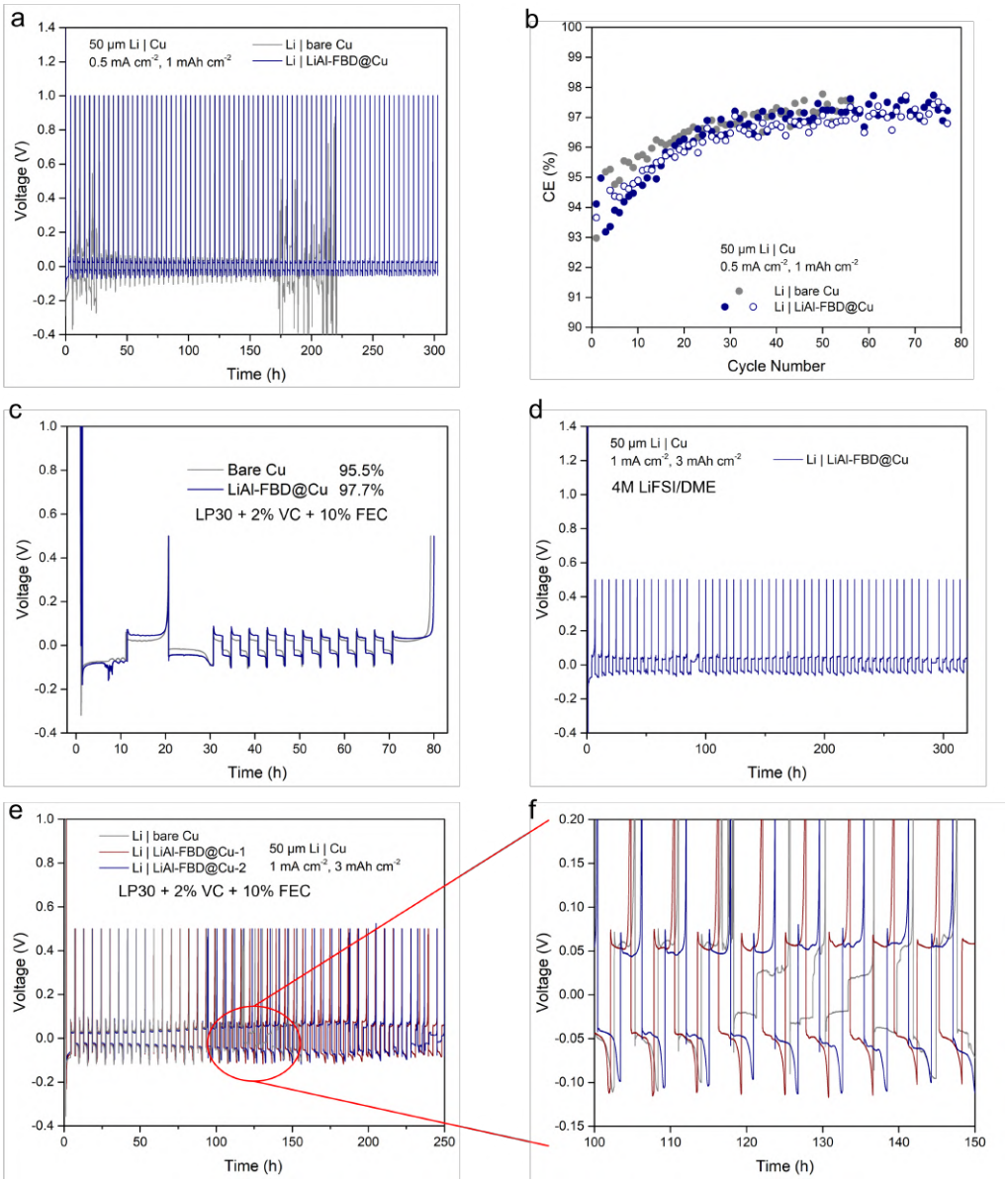


Figure 3.7: (a) Cycling curves of 50-μm-thick Li | bare Cu and 50-μm-thick Li | LiAl-FBD@Cu half cells using 1M LiPF6 in EC/DMC (LP30) + 2% VC + 10% FEC electrolyte. (b) CEs of Li | Cu half cells in (a). Replicated results for LiAl-FBD@Cu are shown in (b). (c) Aurbach protocol [31, 32] test of Li | bare Cu and Li | LiAl-FBD@Cu half cells showing the average CE. (d) Cycling of 50-μm-thick Li | LiAl-FBD@Cu half cell using 4M LiFSI/DME electrolyte at 1 mA cm^{-2} current density and 3 mAh cm^{-2} areal capacity. (e,f) Cycling of 50-μm-thick Li | bare Cu and 50-μm-thick Li | LiAl-FBD@Cu half cells using LP30 + 2% VC + 10% FEC electrolyte at 1 mA cm^{-2} current density and 3 mAh cm^{-2} areal capacity.

Li | bare-Cu cell for the initial $\sim$ 10 cycles (Fig. 3.7b), probably a consequence of the artifact caused by the voltage fluctuation at the initial cycling stage (Fig. 3.7a). By considering the voltage plateaux noises, the Aurbach CE protocol [31, 32] tests and the Li | Cu half-cell cycling under other conditions (see Fig. 3.7c to 3.7f), the superior performance for LiAl-FBD@Cu over the Li | bare-Cu ones is finally confirmed.

3.5.3 Li-NMC full cells

In order to investigate the effectiveness of LiAl-FBD coating under more realistic conditions, we finally assembled practical Li metal full batteries. Thin Li foil (50 μm thick), commercial lithium nickel manganese cobalt (NMC) oxide cathode sheets with high loadings (2 mAh cm^{-2} NMC532 from commercial source and 3.5 mAh cm^{-2} NMC811 provided by Hyundai Motor Company), lean electrolyte amount (30 or 10 μL/cell, i.e., electrolyte-to-cathode ratio was 15 μL mAh^{-1} for NMC532 and 2.8 μL mAh^{-1} for NMC811), and high cycling current (0.6 mA cm^{-2} for NMC532 cells and 1 mA cm^{-2} for NMC811 ones) were implemented here to faithfully replicate testing conditions.

First, we used a commercial carbonate electrolyte (LP30 + 2% VC + 10% FEC). Figure 3.8a shows that the bare-Li full cell suffered from a sharp decay at $\sim$100 cycles; this phenomenon was associated with electrolyte depletion [33] resulting from the unstoppable Li/electrolyte parasitic reactions. As plotted in Fig. 3.8b, the LiAl-FBD@Li | NMC532 full cells possessed stable cycle life, and over 60% of original capacity was retained after 200 cycles. No drastic decrease in capacity was observed, thus indicating the LiAl-FBD ASEI effectively protected the Li metal anode by preventing continuous corrosion or electrolyte depletion [33]. It is worth noting that the manifest difference in cycling behavior between the LiAl-FBD@Li

cell and the bare one well conforms with the EIS evolution (Fig. 3.3a and 3.3b) and XPS (Fig. 3.4a to 3.4d) results. Consistent with the capacity retention trend, the CE of bare Li | NMC532 full cell experienced severe fluctuations from 100 cycles, while the CE was kept stable (∼100%) throughout the whole cycle life (Fig. 3.8b).

To further push the cycling performance, high-concentration ether-based electrolyte, 4M LiFSI/DME27, was employed. As shown in Fig. 3.8c and 3.8d, the bare Li | NMC811 cell experienced a sudden capacity plunge after ∼130 cycles, exactly when the full-cell CE started to significantly fluctuate (Fig. 3.8c and 3.8d). By contrast, the LiAl-FBD@Li | NMC811 cell was stably cycled for ∼200 cycles followed by gradual capacity fading until ∼250 cycles (Fig. 3.8c). Such a gradual decay is consistent with the LiAl-FBD@Li | NMC532 cell results, and proves once again the protection effect of the LiAl-FBD ASEI. The CE of the LiAl-FBD cell was maintained at ∼100% for >230 cycles before any fluctuation occurred (Fig. 3.8d). When other electrolyte recipes and cycling conditions were used, the LiAl-FBD@Li cells all showed better performance than bare ones (Supplementary Figures 5.3, Fig. 3.8).

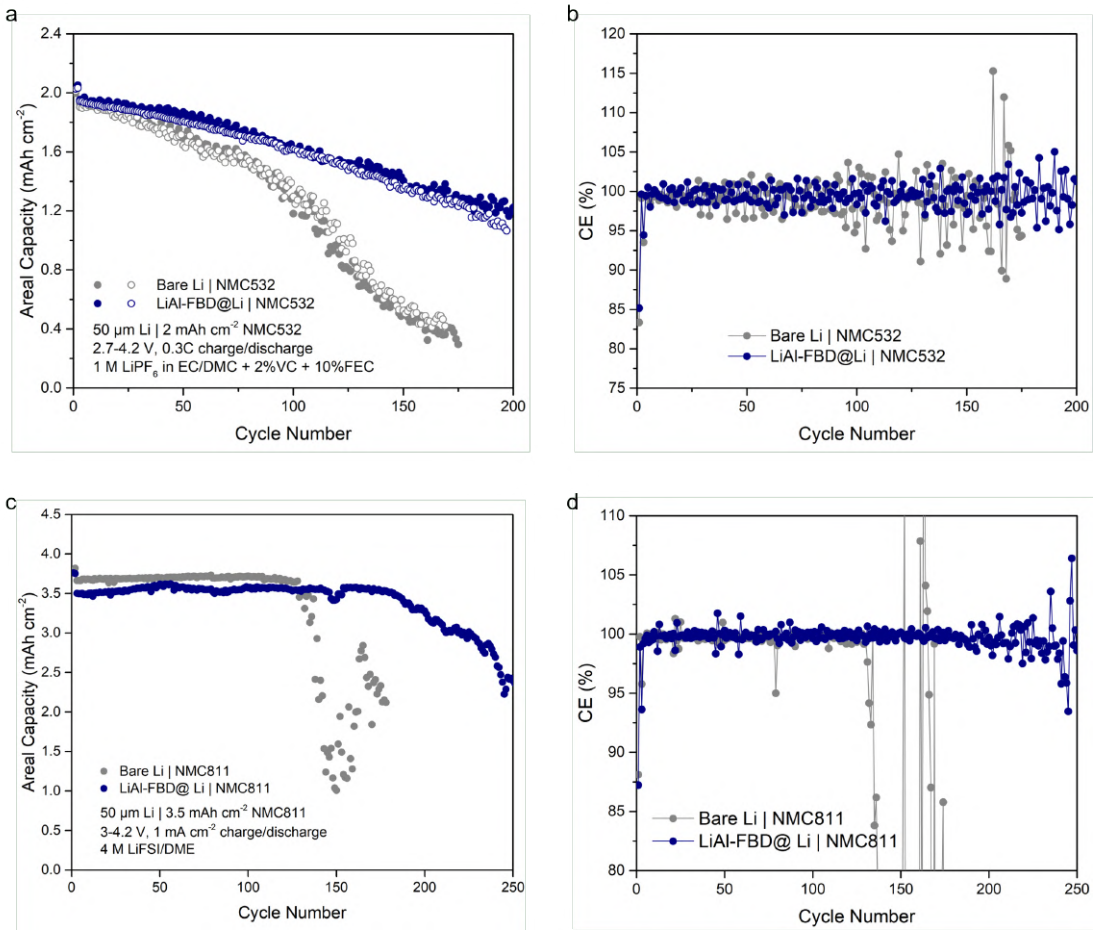
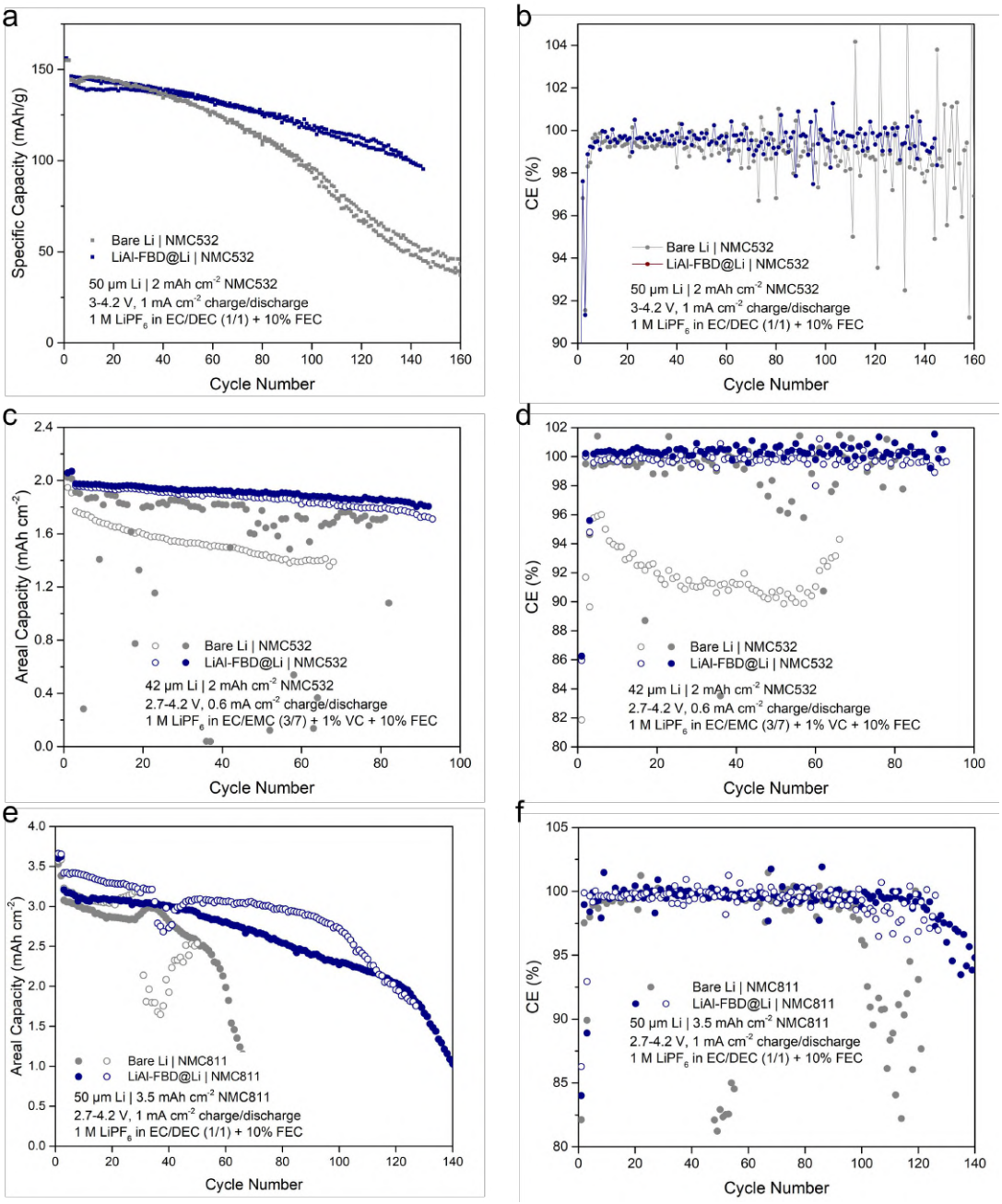


Figure 3.8: (a,b) Full cell performance and corresponding CE evolution using 50-μm-thick Li, commercial NMC532 cathode sheet, and commercial carbonate electrolyte. (c,d) Full cell performance and corresponding CE evolution using 50-μm-thick Li, industrial NMC811 cathode sheet, and high-concentration ether electrolyte. Replicated results for bare Li and LiAl-FBD@Li cells are shown here, in Fig. 3.8 and Supporting Figures, 5.12.


a
Specific Capacity (mAh/g)
Cycle Number
Bare Li | NMC532
LiAl-FBD@Li | NMC532
50 µm Li | 2 mAh cm-2 NMC532
3-4.2 V, 1 mA cm-2 charge/discharge
1 M LiPF6 in EC/DEC (1/1) + 10% FEC
b
CE (%)
Cycle Number
Bare Li | NMC532
LiAl-FBD@Li | NMC532
50 µm Li | 2 mAh cm-2 NMC532
3-4.2 V, 1 mA cm-2 charge/discharge
1 M LiPF6 in EC/DEC (1/1) + 10% FEC
c
Areal Capacity (mAh cm-2)
Cycle Number
Bare Li | NMC532
LiAl-FBD@Li | NMC532
42 µm Li | 2 mAh cm-2 NMC532
2.7-4.2 V, 0.6 mA cm-2 charge/discharge
1 M LiPF6 in EC/EMC (3/7) + 1% VC + 10% FEC
d
CE (%)
Cycle Number
Bare Li | NMC532
LiAl-FBD@Li | NMC532
42 µm Li | 2 mAh cm-2 NMC532
2.7-4.2 V, 0.6 mA cm-2 charge/discharge
1 M LiPF6 in EC/EMC (3/7) + 1% VC + 10% FEC
e
Areal Capacity (mAh cm-2)
Cycle Number
Bare Li | NMC811
LiAl-FBD@Li | NMC811
50 µm Li | 3.5 mAh cm-2 NMC811
2.7-4.2 V, 1 mA cm-2 charge/discharge
1 M LiPF6 in EC/DEC (1/1) + 10% FEC
f
CE (%)
Cycle Number
Bare Li | NMC811
LiAl-FBD@Li | NMC811
50 µm Li | 3.5 mAh cm-2 NMC811
2.7-4.2 V, 1 mA cm-2 charge/discharge
1 M LiPF6 in EC/DEC (1/1) + 10% FEC

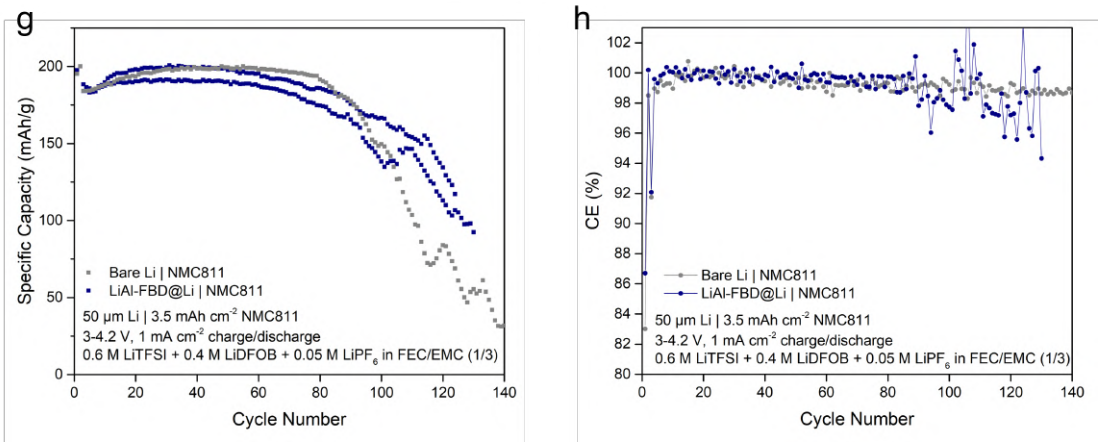


Figure 3.8: Long-term cycling of thin-Li | NMC full cells under different conditions. (a,b) 50-μm-thick Li | 2 mAh cm^{-2} NMC532 using LP40 + 10% FEC under C/2 cycling. (c,d) 42-μm-thick Li | 2 mAh cm^{-2} NMC532 using LP57 + 1% VC + 10% FEC under 0.3C cycling. (e,f) 50-μm-thick Li | 3.5 mAh cm^{-2} NMC811 using LP40 + 10% FEC under 0.3C cycling. (g,h) 50-μm-thick Li | 3.5 mAh cm^{-2} NMC811 using 0.6 M LiTFSI + 0.4 M LiDFOB + 0.05 M LiPF6 in FEC/EMC (3/7) under 0.3C cycling. Replicated cells are shown here.

Chapter 4

Conclusions and Outlook

In summary, we designed and synthesized a mechanically robust artificial solid electrolyte interface (ASEI), LiAl-FBD, that can be solution-processed easily on Li foil. The single crystal structure was solved and demonstrated to be $Li_3Al_3(FBD)_6(DME)_3$, in which Al^{3+} ions were bridged by FBD^{2-} ligands to form the anion-cluster while Li^+ ions were loosely bound and located at the periphery. Such a feature, along with high Li^+ content due to short ligands, enabled fast ion transport. In addition, the highly fluorinated ligands endowed the ASEI with electrolyte-phobicity. Careful characterizations such as nanoindentation, XPS, SEM, EIS, Li | Li symmetric cell cycling and Li metal CE showed that LiAl-FBD is a mechanically-strong, electrolyte-blocking, and ion-conductive coating to well protect the Li metal anode. The Li metal batteries using LiAl-FBD coated thin Li foil, commercial or industrial NMC high-voltage high-loading cathodes, and lean electrolyte condition showed superior cycling performance than bare Li cells, confirming the practicality of using this solution-processable ASEI in realistic Li metal batteries.

Bibliography

[1] Jun Liu et al. "Pathways for practical high-energy long-cycling lithium metal batteries". In: *Nature Energy* 4.3 (2019), pp. 180–186.

[2] Yuliang Cao et al. "Bridging the academic and industrial metrics for next-generation practical batteries". In: *Nature nanotechnology* 14.3 (2019), pp. 200–207.

[3] Xin-Bing Cheng et al. "A review of solid electrolyte interphases on lithium metal anode". In: *Advanced science* 3.3 (2016), p. 1500213.

[4] MD Tikekar et al. *Design principles for electrolytes and interfaces for stable lithium-metal batteries. Nat Energy 1: 16114*. 2016.

[5] Zhiao Yu et al. "A dynamic, electrolyte-blocking, and single-ion-conductive network for stable lithium-metal anodes". In: *Joule* 3.11 (2019), pp. 2761–2776.

[6] Mun Sek Kim et al. "Langmuir-Blodgett artificial solid-electrolyte interphases for practical lithium metal batteries". In: *Nature Energy* 3.10 (2018), pp. 889–898.

[7] Kai Liu et al. "Materials for lithium-ion battery safety". In: *Science advances* 4.6 (2018), p. 9820.

[8] Dingchang Lin, Yayuan Liu, and Yi Cui. “Reviving the lithium metal anode for high-energy batteries”. In: *Nature nanotechnology* 12.3 (2017), pp. 194–206.

[9] Wu Xu et al. “Lithium metal anodes for rechargeable batteries”. In: *Energy & Environmental Science* 7.2 (2014), pp. 513–537.

[10] Kai Liu et al. “Lithium metal anodes with an adaptive “solid-liquid” interfacial protective layer”. In: *Journal of the American Chemical Society* 139.13 (2017), pp. 4815–4820.

[11] Xiulin Fan and Chunsheng Wang. “High-voltage liquid electrolytes for Li batteries: progress and perspectives”. In: *Chemical Society Reviews* (2021).

[12] Benjamin Flamme et al. “Guidelines to design organic electrolytes for lithium-ion batteries: environmental impact, physicochemical and electrochemical properties”. In: *Green Chemistry* 19.8 (2017), pp. 1828–1849.

[13] Shuhong Jiao et al. “Stable cycling of high-voltage lithium metal batteries in ether electrolytes”. In: *Nature Energy* 3.9 (2018), pp. 739–746.

[14] Ziqi Zeng et al. “Non-flammable electrolytes with high salt-to-solvent ratios for Li-ion and Li-metal batteries”. In: *Nature Energy* 3.8 (2018), pp. 674–681.

[15] Jeffrey W Fergus. “Ceramic and polymeric solid electrolytes for lithium-ion batteries”. In: *Journal of Power Sources* 195.15 (2010), pp. 4554–4569.

[16] Junheng Li et al. “Polymers in Lithium-Ion and Lithium Metal Batteries”. In: *Advanced Energy Materials* 11.15 (2021), p. 2003239.

[17] Nian-Wu Li et al. “An artificial solid electrolyte interphase layer for stable lithium metal anodes”. In: *Advanced materials* 28.9 (2016), pp. 1853–1858.

[18] Hao Chen et al. “Uniform high ionic conducting lithium sulfide protection layer for stable lithium metal anode”. In: *Advanced Energy Materials* 9.22 (2019), p. 1900858.

[19] Hansen Wang et al. “Lithium metal anode materials design: interphase and host”. In: *Electrochemical Energy Reviews* 2.4 (2019), pp. 509–517.

[20] Fei Ding et al. “Dendrite-free lithium deposition via self-healing electrostatic shield mechanism”. In: *Journal of the American Chemical Society* 135.11 (2013), pp. 4450–4456.

[21] Quan Pang, Laidong Zhou, and Linda F Nazar. “Elastic and Li-ion–percolating hybrid membrane stabilizes Li metal plating”. In: *Proceedings of the National Academy of Sciences* 115.49 (2018), pp. 12389–12394.

[22] Shuya Wei et al. “Electrochemical interphases for high-energy storage using reactive metal anodes”. In: *Accounts of chemical research* 51.1 (2018), pp. 80–88.

[23] Guangyuan Zheng et al. “High-performance lithium metal negative electrode with a soft and flowable polymer coating”. In: *ACS Energy Letters* 1.6 (2016), pp. 1247–1255.

[24] Sabrina Fischer et al. “A Metal–Organic Framework with Tetrahedral Aluminate Sites as a Single-Ion Li+ Solid Electrolyte”. In: *Angewandte Chemie International Edition* 57.51 (2018), pp. 16683–16687.

[25] Zhiao Yu et al. “A solution-processable artificial solid electrolyte interphase for practical lithium metal batteries”. In: *Manuscript in preparation* (2022).

[26] Zhiao Yu, Yi Cui, and Zhenan Bao. “Design principles of artificial solid electrolyte interphases for lithium-metal anodes”. In: *Cell Reports Physical Science* 1.7 (2020), p. 100119.

[27] Yayuan Liu et al. “An ultrastrong double-layer nanodiamond interface for stable lithium metal anodes”. In: *Joule* 2.8 (2018), pp. 1595–1609.

[28] Yue Gao et al. “Polymer–inorganic solid–electrolyte interphase for stable lithium metal batteries under lean electrolyte conditions”. In: *Nature materials* 18.4 (2019), pp. 384–389.

[29] Yuming Zhao et al. “Stable Li metal anode by a hybrid lithium polysulfidophosphate/polymer cross-linking film”. In: *ACS Energy Letters* 4.6 (2019), pp. 1271–1278.

[30] Zhiao Yu et al. “Molecular design for electrolyte solvents enabling energy-dense and long-cycling lithium metal batteries”. In: *Nature Energy* 5.7 (2020), pp. 526–533.

[31] Doron Aurbach, Yosef Gofer, and Jacob Langzam. “The correlation between surface chemistry, surface morphology, and cycling efficiency of lithium electrodes in a few polar aprotic systems”. In: *Journal of the Electrochemical Society* 136.11 (1989), p. 3198.

[32] Brian D Adams et al. “Accurate determination of Coulombic efficiency for lithium metal anodes and lithium metal batteries”. In: *Advanced Energy Materials* 8.7 (2018), p. 1702097.

[33] Chaojiang Niu et al. “Balancing interfacial reactions to achieve long cycle life in high-energy lithium metal batteries”. In: *Nature Energy* 6.7 (2021), pp. 723–732.

Chapter 5

Appendix

5.1 Materials

2,2,3,3-Tetrafluoro-1,4-butanediol (FBD) was purchased from SynQuest Laboratories and used as received. 1M lithium aluminum hydride in tetrahydrofuran solution (1M $LiAlH_4$/THF), THF (anhydrous, $\geq$99.9%, inhibitor-free), and vinylene carbonate (VC, 99.5%, acid $<$200 ppm, H_2O $<$100 ppm) were purchased from Sigma-Aldrich and used as received. 1,2-Dimethoxyethane (anhydrous, 99.5%) was purchased from ACROS Organics and used as received. Other commercial reactants were purchased from Sigma-Aldrich and used without further purification.

5.1.1 Battery Materials

1M $LiPF_6$ in EC/DMC (LP30), 1M $LiPF_6$ in EC/EMC (LP57) and 1M $LiPF_6$ in EC/DEC electrolyte (LP40) were purchased from Gotion. EMC, VC and LiDFOB were purchased from Sigma. FEC was purchased from Guangdong Canrd. LiTFSI was provided by Solvay. One layer of Celgard 2325 (25 μm thick PP/PE/PP) or alumina-coated PE (provided by Hyundai Motor Company) was used as separator. Thick Li foil (750 μm thick) was purchased from Alfa Aesar. Thin Li

foil ($\sim$ 50 μm thick) was purchased from China Energy Lithium. Another type of thin Li foil ($\sim$ 42 μm thick) was provided by Hydro-Québec. Copper current collector (25 μm, 99.8% metals basis) was purchased from Alfa Aesar. Single-side coated $LiNi_{0.5}Mn_{0.3}Co_{0.2}O_2$ (NMC532) sheets with $\sim$ 2 mAh cm^{-2} capacity loading were purchased from MTI and $LiNi_{0.8}Mn_{0.1}Co_{0.1}O_2$ (NMC811) sheets with $\sim$ 3.5 mAh cm^{-2} capacity loading were provided by Hyundai Motor Company. Other battery materials, such as 2032-type coin cell cases, springs, and spacers were all purchased from MTI.

5.2 Methods

5.2.1 Synthesis of LiAl-FBD

In an argon-filled glovebox with sub-ppm O_2 (<1 ppm) and H_2O (<0.1 ppm) level (MBRAUN), to an 8 mL vial were added 162 mg FBD and 3 mL DME. Under stirring, 500 μL 1M $LiAlH_4$/THF was added dropwise into the vial. After stirring at room temperature overnight, the yielding solution was filtered through 0.45 μm PTFE filter into 8 mL vial, to obtain $\sim$ 50 mg mL^{-1} LiAl-FBD/DME solution. For single crystals, the LiAl-FBD solution was heated to 80 °C for 6 h to slowly evaporate part of the solvents. After cooling down to room temperature, the crystals were precipitated and transferred into anhydrous hexane for storing.

5.2.2 Fabrication of LiAl-FBD coated Li and Cu

In an argon-filled glovebox with sub-ppm O_2 and H_2O level (Vigor Tech), the coated Cu working electrodes or coated thin Li foils were fabricated with dip-coating method as follows. First, Li foils were punched into 1.0 (for Li | Li and LiCu

cells) or 1.98 (for Li | NMC full cells) cm^2 round disks, while Cu foils were punched into 2.1 (for Li | Cu half cells) cm^2. Then they were dipped into $\sim$ 50 mg mL^{-1} LiAl-FBD in DME solution for 1 min and then lifted out. The remaining solution on Li was immediately but gently wiped out with Kimwipes (KIMTECH) until dry yet sticky surface formed.

5.2.3 Nanoindentation tests

For the nanoindentation measurement of Young's modulus and hardness, LiAl-FBD crystal was fixed using epoxy glue onto a Si wafer and the surface was polished finely. The as-prepared Si wafer was later mounted onto an aluminum puck using graphite paste. A Berkovich tip with a dynamic indentation method was used to probe the modulus and hardness of the crystal surface, and the measurement was performed on a Nanomechanics iNano Nanoindenter.

5.2.4 Material Characterizations

^{1}H-, ^{13}C-, and ^{19}F-NMR spectra were recorded on a Varian Mercury 400 MHz NMR spectrometer and ^{7}Li-NMR spectra were recorded on a UI 500 MHz NMR spectrometer at room temperature. A FEI Magellan 400 XHR SEM and a Thermo Fisher Scientific Apreo S LoVac were used for SEM and EDS characterizations. XPS profiles were collected by PHI VersaProbe 1 Scanning XPS Microprobe. The samples were transferred for XPS using a sample transfer vessel that prevented air exposure at any time. Before XPS measurement, the artificial SEIs coated or bare Li was soaked in the electrolyte for 4 days, and then washed with DME for 30 seconds to remove electrolyte and coating layers.

5.2.5 Electrochemical Measurements

All battery components used in this work were commercial large-scale products and electrochemical testing was all carried out in 2032-type coin cell configuration. The EIS measurements were carried out on a Biologic VMP3 system. The cycling tests for half cells and full cells were carried out on an Arbin system. The EIS measurements were taken over a frequency range from 7 MHz to 100 mHz. For Li | Cu half-cell CE cycling tests, ten pre-cycles between 0 and 1 V were initialized to clean Cu electrode surface, and then cycling was done by depositing 1 (or 3) mAh cm^{-2} of Li onto Cu electrode followed by stripping to 1 V. The average CE is calculated by dividing the total stripping capacity by the total deposition capacity after the formation cycle.

For Aurbach CE test, a standard protocol was followed [31, 32]:

(1) perform one initial formation cycle with Li deposition of 5 mAh cm^{-2} on Cu under 0.5 mA cm^{-2} current density and stripping to 1 V;

(2) deposit 5 mAh cm^{-2} Li on Cu under 0.5 mA cm^{-2} current density as Li reservoir;

(3) repeatedly strip/deposit Li with 1 mAh cm^{-2} under 0.5 mA cm^{-2} current density for 10 cycles;

(4) strip all Li to 1 V.

For the Li | NMC full cell study, NMC532 and NMC811 cathode sheets were used and stored in argon-filled glovebox as received. After the first two activation cycles at C/10 charge/discharge, the cells were cycled at different current densities and voltage ranges.

5.3 Supplementary Figures

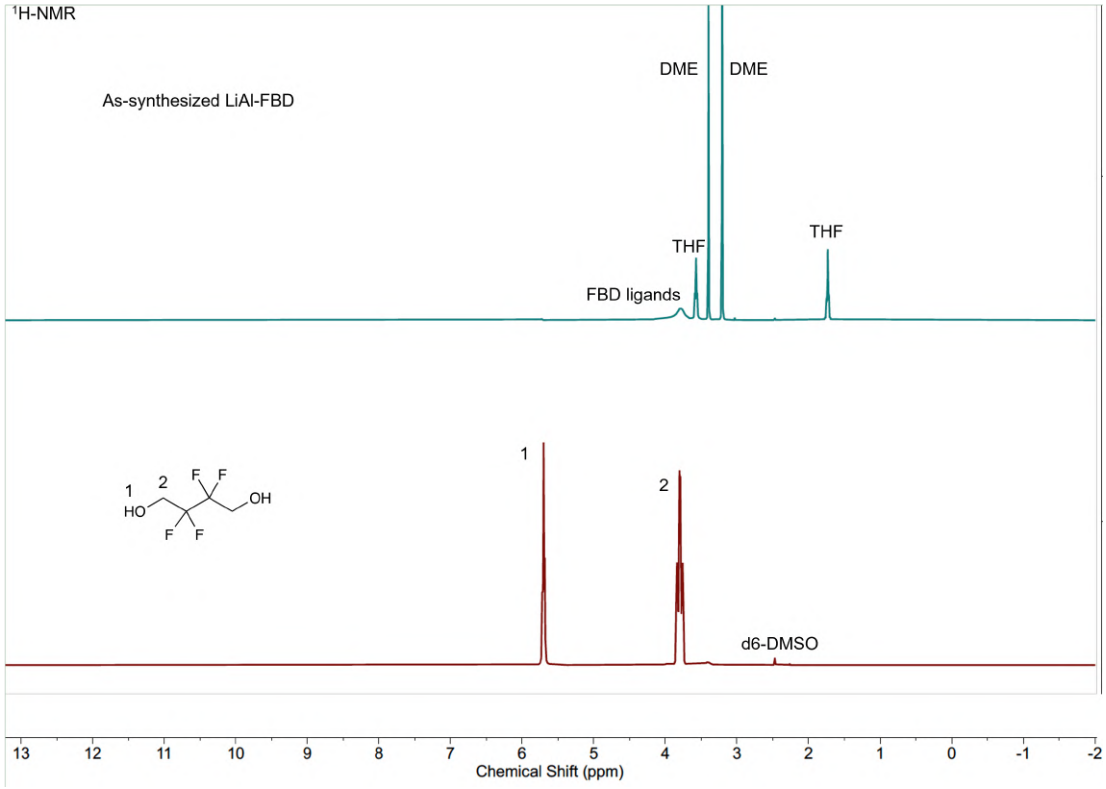


Figure 5.1: ^{1}H-NMR of LiAl-FBD (upper) and FBD (bottom).

Note: After the synthesis, the FBD diol was successfully deprotonated (the disappearance of peak 1) and the peak 2 got broadened. The remaining THF from $LiAlH_4$ solution and the DME solvent were also observed in the LiAl-FBD sample.

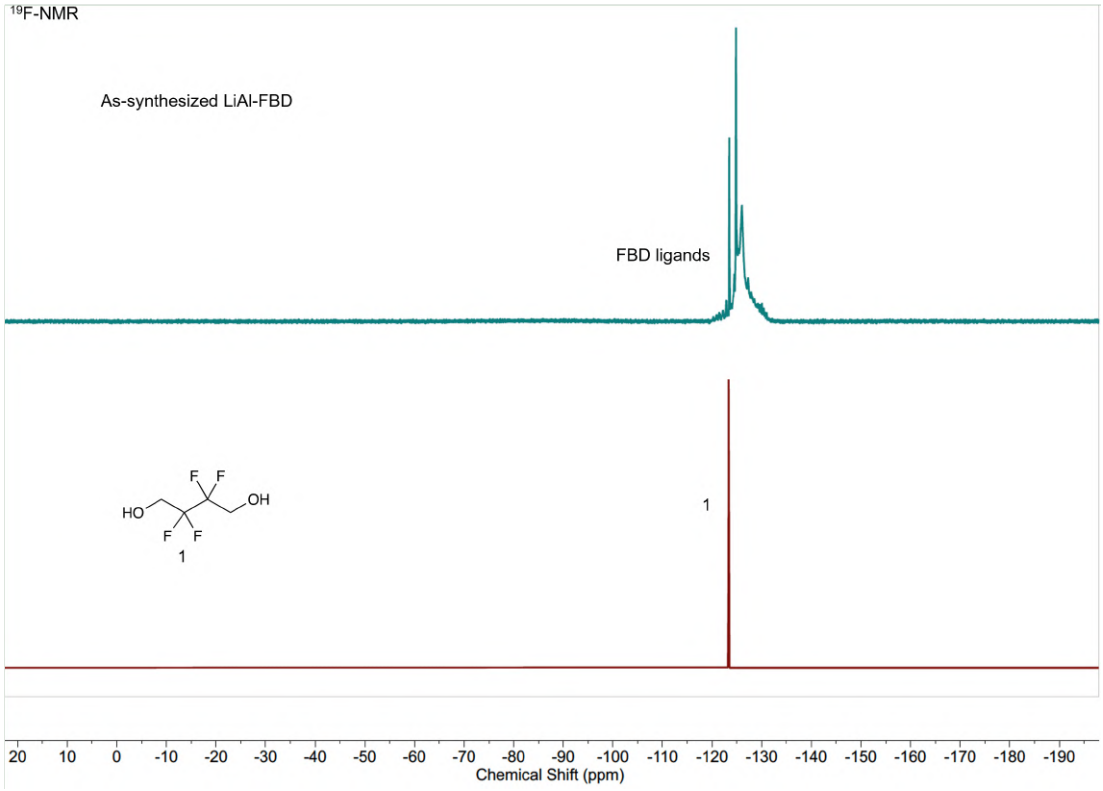


Figure 5.2: ^{19}F-NMR of LiAl-FBD (upper) and FBD (bottom).

Note: After the synthesis, the ^{19}F signal on FBD ligands got broadened, showing different chemical environments in the LiAl-FBD material.

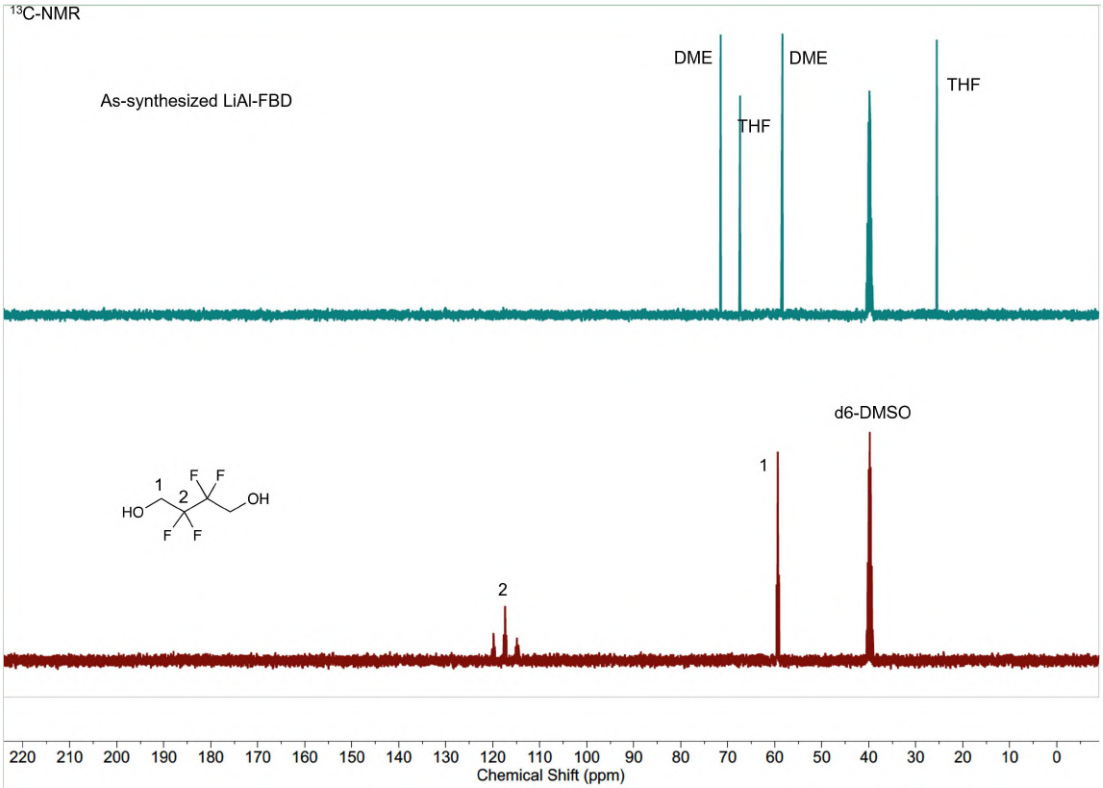


Figure 5.3: ^{13}C-NMR of LiAl-FBD (upper) and FBD (bottom).

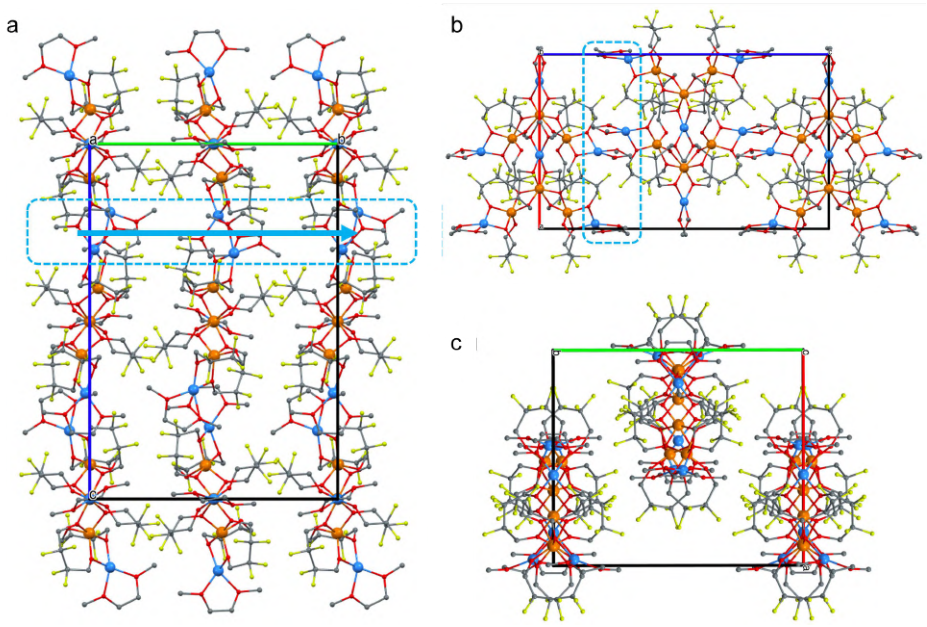


Figure 5.4: Crystal structure of $Li_3Al_3(FBD)_6(DME)_3$ viewing from a- (a), b- (b), and c- (c) axis [25].

Note: The potential Li+ ion transport pathway was labeled in light blue arrow in (a) and (b). Particularly, a sterically favored Li^+ transport channel can be observed from (b). The space is only occupied by a fewer species and Li^+-DME is expected to readily hop.

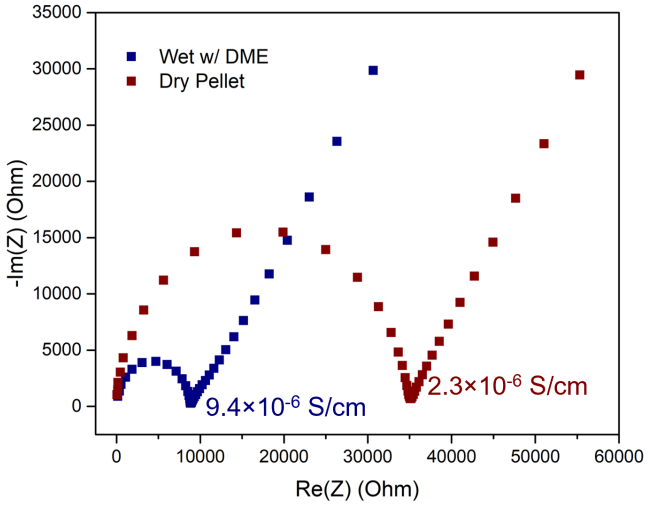


Figure 5.5: Nyquist plot of electrochemical impedance of dry and wet LiAl-FBD pellet. The wet pellet was prepared by adding 10 w.t.% DME solvent as the plasticizer into the dry pellet.

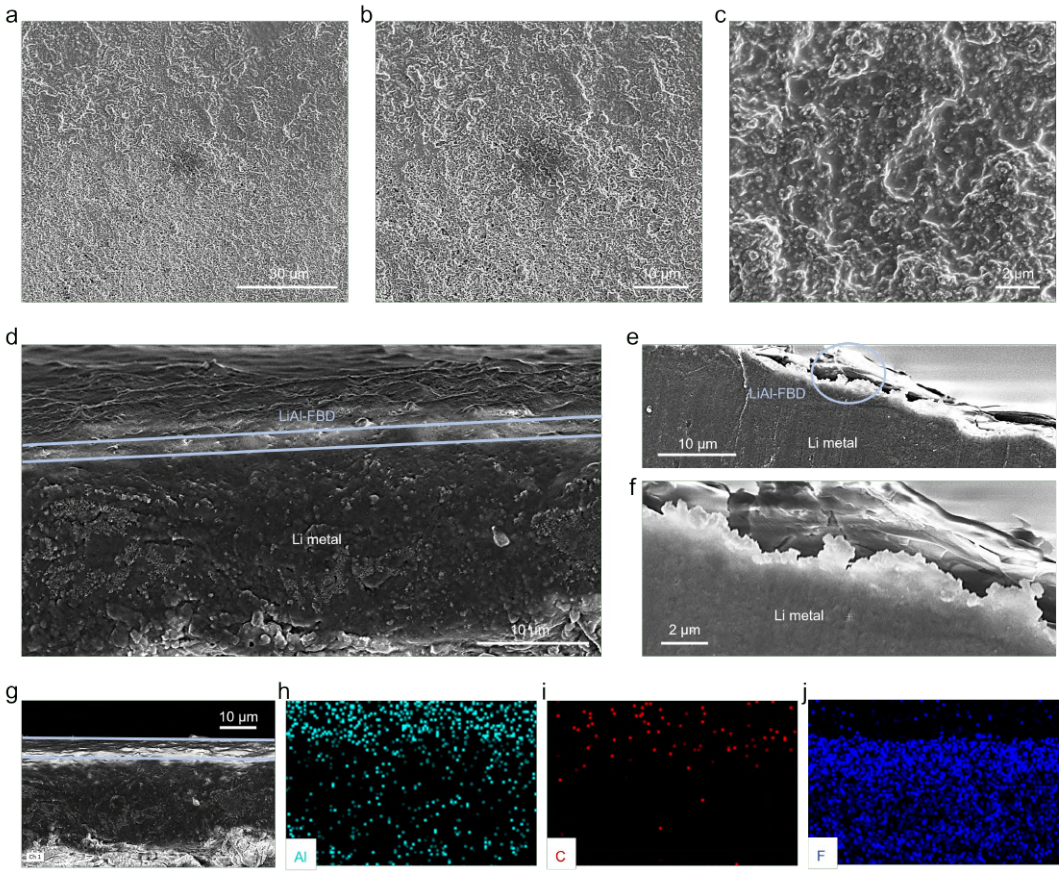


Figure 5.6: (a-c) Top-view SEM images with different scales showing the conformal morphology of LiAl-FBD coating. (d-f) Cross-sectional SEM images showing the thickness (∼500 nm) of LiAl-FBD coating on Li foil. (g-j) EDS of LiAl-FBD coating on 50-μm-thick Li metal foil: Al (h), C (i), and F (j).

Note: The samples used here were Li foils directly dip-coated by LiAl-FBD solution. As shown from the top-view SEM images (a-c), the LiAl-FBD showed conformal coating that covered Li metal surface at all different scales. The cross-sectional SEM images showed that the coating thickness is around 500 nm. The EDS results further confirmed the existence and location of LiAl-FBD: the characteristic elements in LiAl-FBD coating layer such as Al, C and F were concentrated around the coating area. Small amount of signal noise/contamination showed up around the Li metal foil area, which mainly originated from the sample preparation (scissors cutting).

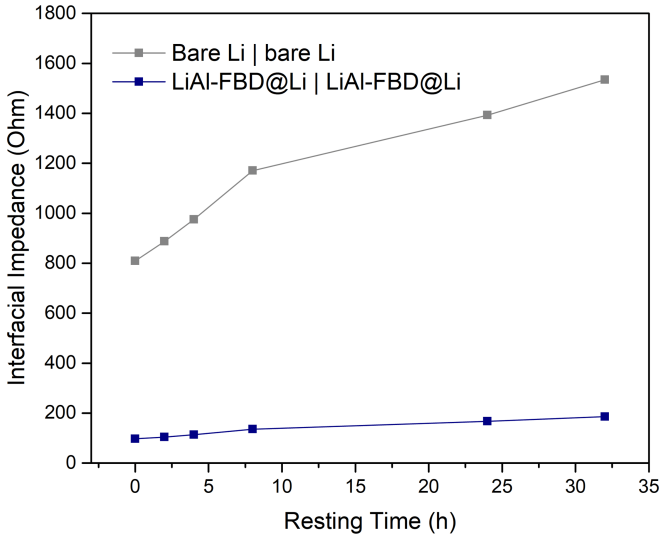


Figure 5.7: Interfacial impedance evolution of bare Li | bare Li and LiAl-FBD@Li | LiAl-FBD@Li symmetric cells over resting time, extracted from Fig. 3.3a and 3.3b.

Note: The absolute values of impedance were much lower for LiAl-FBD coated Li symmetric cell, and the increasing trend of impedance was suppressed as well.

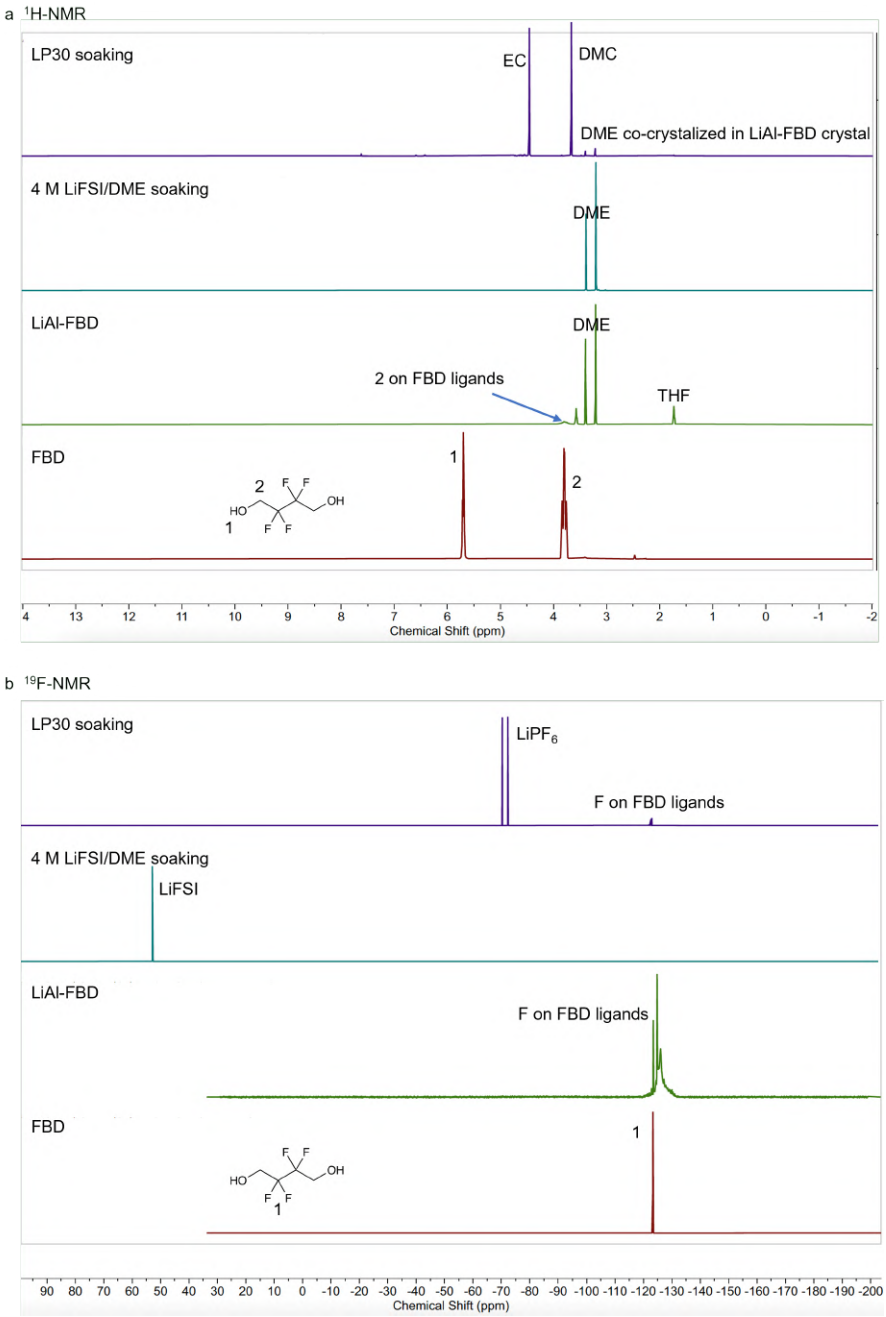


Figure 5.8: ^{1}H- (a) and ^{19}F- (b) NMR of the solutions after LiAl-FBD crystal soaking in LP30 or 4M LiFSI/DME electrolytes for ∼24 h.

Note: Overall, the LiAl-FBD was stable after soaking in the electrolytes we used in this work, with the electrolyte solutions containing few LiAl-FBD species as well.

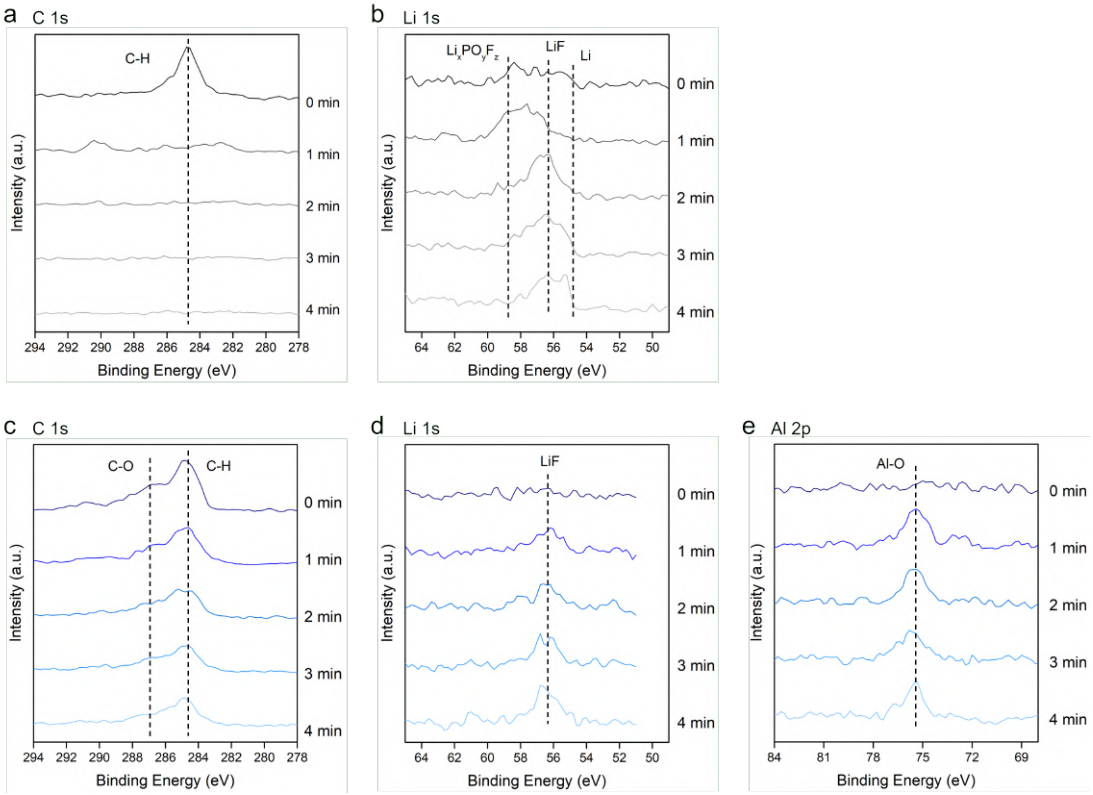


Figure 5.9: (a,b) XPS C1s (a) and Li1s (b) of bare Li. (c-e) XPS C1s (c), Li1s (d) and Al2p (e) of LiAl-FBD@Li.

Note: Compared to the elemental information on bare Li surface, the LiAl-FBD@Li surface showed more C-O in C1s spectra and vertically uniform distribution of LiF species in F1s spectra, both of which are critical features for favorable Li metal protection. The Al2p spectra showed Al-O bonds which derived from LiAl-FBD coating.

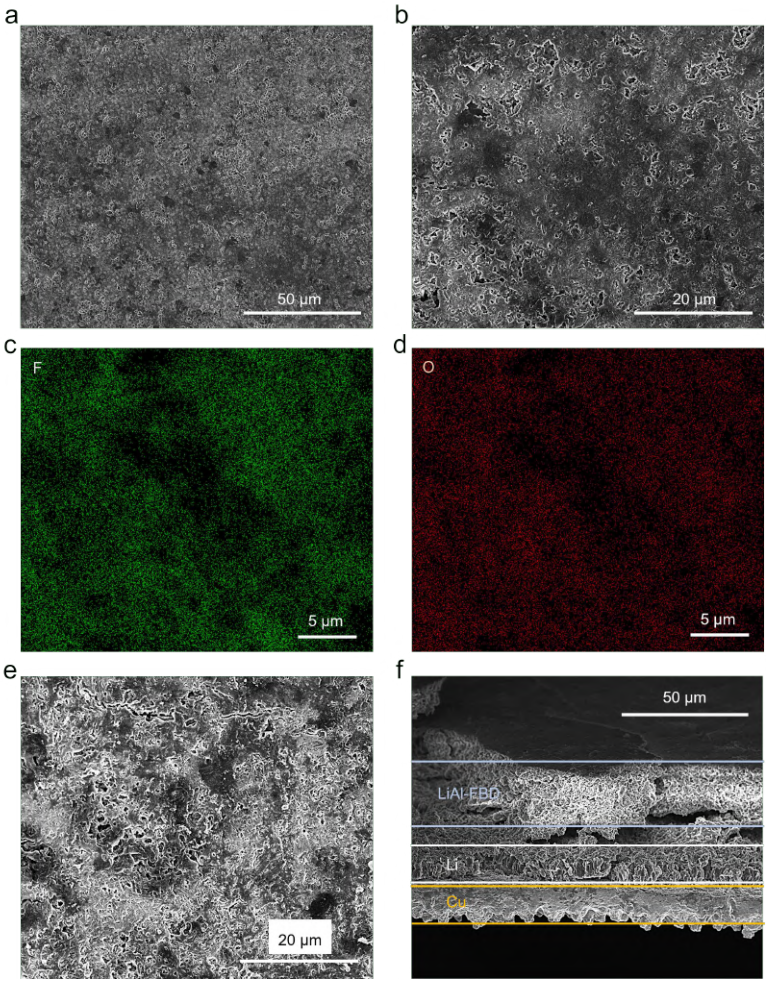


Figure 5.10: (a,b) SEM images of LiAl-FBD@Cu (with Li deposits underneath) after 10 cycles in the Li | Cu half cell. (c,d) EDS mapping of F (c), and O (d) element. (e,f) SEM images (top-view for e and cross-sectional for f) of LiAl-FBD@Cu (with Li deposits underneath) after 50 cycles in the Li | Cu half cell.
Carbonate electrolyte LP30 + 2% VC + 10% FEC was used here. The samples were prepared by cycling 1 mAh cm^{-2} Li at 0.5 mA cm^{-2} current density on either bare Cu or LiAl-FBD@Cu for either 10 or 50 cycles, followed by depositing 1 mAh cm^{-2} Li at 0.5 mA cm^{-2} current density on the Cu substrate (underneath LiAl-FBD coating).

Note: The EDS colors scheme of different elements are different from those used in Fig. 3.5j, 3.5k, 3.5l since different SEM/EDS instruments were used. As shown in (f), the LiAl-FBD coating (top part between the light blue lines) was peeled off (the layer was curled up due to peeling) and the Li deposits (deposited after 50 cycles) were densely packed underneath the LiAl-FBD layer, showing its protection function even after long-term cycling.

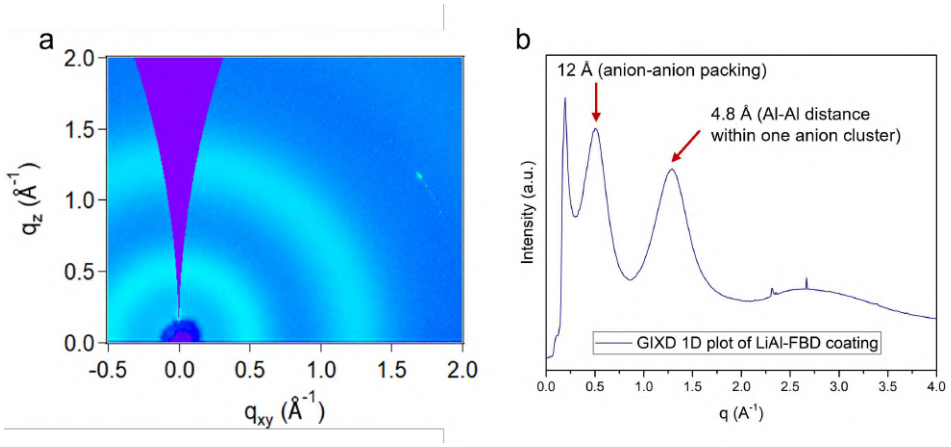


Figure 5.11: (a,b) Grazing-incidence wide-angle X-ray scattering (GIWAXS) results of LiAl-FBD coating on Si wafer [25].

Note: The GIWAXS analysis supports the polarized optical microscope results (Fig. 3.2c and 3.2d) by showing distinguished anion packing peak at ∼12 Å(q ∼0.52 Å^{-1}).

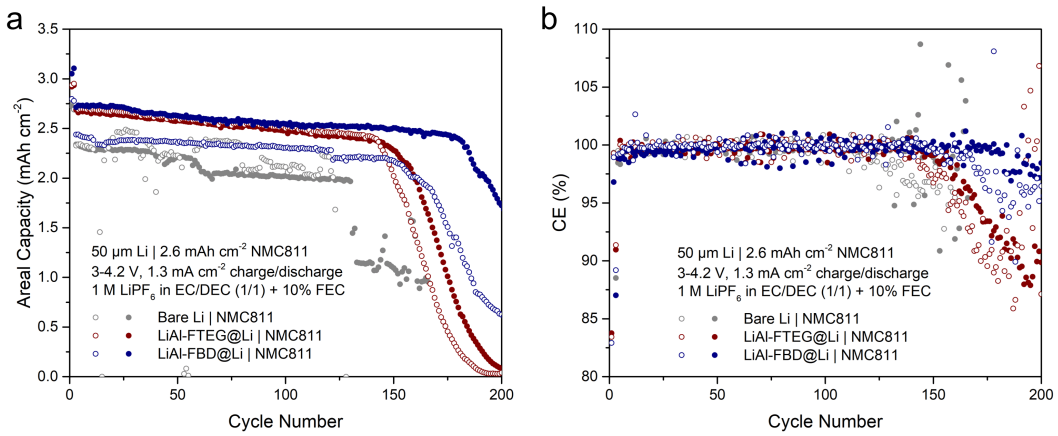


Figure 5.12: Comparison of cycling performance of thin-Li | NMC full cells: bare Li, LiAl-FTEG@Li, and LiAl-FBD@Li. 50-μm-thick Li | 2.6 mAh cm^{-2} NMC811 using LP40 + 10% FEC under 0.5C cycling. Replicated cells are shown here.

Note: Proposed in a previous report [5], LiAl-FTEG is a dynamic, single-ion-conductive and electrolyte-blocking coating material with with low modulus (storage modulus around 1-10 MPa by rheological measurement). LiAl-FBD coating shows slightly better cycling stability than bare control or LiAl-FTEG@Li, which can be attributed to the mechanical strength of LiAl-FBD (Young's modulus around 30-40 GPa by nanoindentation).